Quantitative profiling of chromatome dynamics reveals a novel role for HP1BP3 in hypoxia-induced oncogenesis

Bamaprasad Dutta[1], Ren Yan[1], Sai Kiang Lim[2], James P. Tam[1] and Siu Kwan Sze[1]*

[1]School of Biological Sciences, Nanyang Technological University, 60 Nanyang Drive, Singapore 637551;
[2]Institute of Medical Biology, A*STAR, 8A Biomedical Grove, Immunos, Singapore 138648

Running title: Hypoxia-induced chromatome promotes tumorigenesis

***Correspondence:**
Siu Kwan SZE, PhD
School of Biological Sciences
Division of Structural Biology and Biochemistry
Nanyang Technological University,
60 Nanyang drive, Singapore 637551
Tel: (+65) 6514-1006
Fax: (+65) 6791-3856
Email: sksze@ntu.edu.sg

Summary

In contrast to the intensely studied genetic and epigenetic changes that induce host cell transformation to initiate tumor development, those that promote malignant progression of cancer remain poorly defined. As emerging evidence suggests that the hypoxic tumor microenvironment could re-model chromatin-associated proteome (chromatome) to induce epigenetic changes and alter gene expression in cancer cells, we hypothesized that hypoxia-driven evolution of the chromatome promotes malignant changes and development of therapy resistance in tumor cells. To test this hypothesis, chromatins were isolated from tumor cells treated with varying conditions of normoxia, hypoxia and re-oxygenation, partially digested with DNase I and analyzed for changes in euchromatin- and heterochromatin-associated proteins using quantitative iTRAQ-based quantitative proteomic approach. We identified a total of 1446 proteins at a high level of confidence, including 819 proteins that were observed to change their chromatin association topology under hypoxic conditions. These hypoxia-sensitive proteins included key mediators of chromatin organization, transcriptional regulation and DNA repair. Furthermore, our proteomic and functional experiments revealed a novel role for the chromatin organizer protein HP1BP3 in mediating chromatin condensation during hypoxia, leading to increased tumor cell viability, radio-resistance, chemo-resistance and self-renewal. Taking together, our findings indicate that HP1BP3 is a key mediator of tumor progression and cancer cell acquisition of therapy-resistant traits, and may thus represent a novel therapeutic target in a range of human malignancies.

Keywords: Hypoxia, tumor progression, cancer steam cells, chromatin, chromatome, euchromatin, heterochromatin, HP1BP3, iTRAQ

Introduction

Microenvironmental hypoxia is a hallmark of rapidly growing solid tumors. In order to overcome the growth restrictions imposed by low-oxygen conditions, cancer cells can promote neovascularization and/or acquire characteristics that increase tumor cell survival, replicative capacity, and potential to undergo metastasis(1). Numerous studies have demonstrated that the hypoxic tumor microenvironment plays a key role in cancer progression towards a metastatic phenotype, and can also promote the acquisition of chemoresistant and radioresistant properties(2-4). Hypoxia inducible factors have already been identified as key mediators of cancer cell development in low-oxygen environments(5), but it is likely that additional molecular mechanisms are also involved in driving the malignant progression of developing tumors.

Tumor progression is thought to be driven by selective pressure on the cancer cells exerted by the hypoxic microenvironment, leading to the clonal evolution of many different cancer cell phenotypes within an individual patient. This combination of increasing diversity and enhanced survival characteristics makes it progressively more difficult to kill all cancer cell types using a single therapeutic strategy. Alternatively, identification and therapeutic disruption of the common mechanisms by which tumor cells progress towards malignancy may offer more effective approaches to cancer treatment. Indeed, the hypoxic tumor microenvironment appears to be a common driver of cancer evolution, since all solid tumors are subjected to hypoxia stress at some point during development as they increase in size but without an immediate increase in oxygen supply. Emerging evidence also suggests that hypoxia contributes to the development of cancer stem cells that exhibit enhanced capacity for self-renewal(6). Together, these data indicate a

critical role for hypoxia-sensitive molecular pathways in promoting cancer progression that it may be possible to target with novel therapies in order to disrupt tumor growth(7).

Hypoxia-inducible factors (HIFs) mediate DNA methylation, histone modification, and host cell expression of regulatory RNAs and chromatin-modeling factors that modulate gene expression in response to low-oxygen conditions(5, 8). However, hypoxia can also induce histone modification and chromatin remodeling via HIF-independent pathways, indicating that additional mechanisms of epigenetic regulation can shape the cellular response to restricted oxygen supplies(9, 10), and potentially increase cell survival and promote angiogenesis in hypoxic conditions(11-14). Hypoxia-induced changes in the composition of the chromatin-associated proteome (chromatome) are therefore likely to alter gene expression and promote clonal evolution in developing tumors. While, better knowledge of chromatome dynamics in low-oxygen conditions is likely to increase our understanding of the molecular events that drive tumor progression, few quantitative proteomic studies of chromatome modulation by hypoxia have been conducted to date.

In the current report, we used partial DNase I digestion together with iTRAQ based quantitative proteomics to analyze the chromatome of A431 cancer cells that had been subjected to hypoxia and re-oxygenation stress. Profiling of both solubilized fraction (euchromatin-associated proteins) and undigested fraction (predominantly heterochromatin-associated proteins) uncovered novel effects of hypoxia on chromatin association topology in growing cancer cells. Furthermore, our proteomic and functional experiments indicated that the chromatin-organizing protein HP1BP3 is a key switch in hypoxia-induced malignant progression and may represent a novel therapeutic target in a wide range of human malignancies.

Materials and methods

Reagents

All reagents were purchased from Sigma-Aldrich unless otherwise indicated. Antibodies against α-tubulin (sc-5286), GAPDH (sc-32233), Ku-70 (sc-17789), and Ku-80 (sc-5280) were from Santa Cruz Biotechnology Inc., CA, USA; anti-histone H2A (ab13923), histone H4 (ab10158), and HP1BP3 (ab98894) from Abcam, Cambridge, UK; and anti-actin (MAB1501) from Millipore, MA, USA.

Cell culture and hypoxia model

A431 squamous carcinoma cells were purchased from ATCC and maintained in DMEM supplemented with 10% FBS, 10000U/ml penicillin, and 10000µg/ml streptomycin. For each experiment, 2×10^6 cells were seeded onto 10cm Petri dishes and grown to 30-40% confluence at 37ºC in 5% CO_2, after which the culture medium was aspirated and replaced with serum-free DMEM. The cells were then placed into a hypoxia chamber and flushed with hypoxic gas (95% N_2, 5% CO_2, <0.1% O_2) at a constant flow rate of 15l/min for a total of 10min before the chamber was sealed and incubated at 37ºC for either 48h or 72h. Alternatively, the cells were cultured under normoxic control conditions (Nx; 21% O_2, 5% CO_2) at 37ºC for 72h duration. In re-oxygenations experiment (Rx), the cells were first incubated in hypoxic conditions for 48h before the culture medium was refreshed and the cells incubated for 24h under normoxia. Experiment was performed in triplicate.

Chromatin isolation and digestion

Chromatin isolation was performed according to the method published by Dutta *et al.* with minor modifications(15). Briefly, 7×10^7 cells were suspended in nuclei extraction buffer A (10mM HEPES pH 7.5, 10mM KCl, 1mM $MgCl_2$, 0.34M sucrose, 0.1% triton X-100, 1mM DTT, and protease inhibitor cocktail from Roche Diagnostics, Mannheim, Germany) and kept on ice for 30min prior to homogenization. The homogenate was centrifuged at 2000×g for 3min at 4°C and the supernatant discarded. The pellet fraction was re-suspended in nuclei extraction buffer B (10mM HEPES pH 7.5, 10mM KCl, 1.5mM $MgCl_2$, 0.34M sucrose, 0.1% NP-40, 1mM DTT, protease inhibitor cocktail) and homogenized for a second time. The homogenate was loaded onto a 2.1M sucrose gradient (10mM HEPES pH 7.5, 10mM KCl, 1.5mM $MgCl_2$, 2.1M sucrose, 1mM DTT, protease inhibitor cocktail) and ultra-centrifuged at 150,000×g for 3h at 4°C using a SW41 rotor with the Optima™ L-100XP Ultra apparatus (Beckman Coulter, CA, USA). After ultra-centrifugation, the supernatant was removed and the chromatin pellet collected from the bottom of the tube. The chromatin pellet was washed with wash buffer (10mM HEPES pH 7.5, 1mM DTT, protease inhibitor cocktail) and collected by centrifugation at 20,000g for 45min at 4°C. The purified chromatin pellet was then suspended in 50µl DNase I digestion buffer (10mM HEPES pH 7.5, 2.5mM $CaCl_2$, 2.5mM $MgCl_2$) and digested with 20U DNase I at 37°C for 60min. Digestion was terminated by adding 1mM EDTA and the supernatant (fraction S) was collected by centrifugation at 20,000g at 4°C for 30min. The remaining undigested pellet (fraction P) was dissolved in 2% SDS solution. The protein contents of the supernatant and pellet fractions were subsequently quantified by 2-D Quant Kits (Amersham Biosciences, USA). Digestion experiment were performed for three biological replicates and the digests obtain from three replicates were pooled together prior to in-gel digestion.

In-gel digestion and iTRAQ labeling

For each sample, 150µg of protein was loaded onto a 12.5% SDS-PAGE gel followed by electrophoresis for 15min at 80V. Sample lanes were cut into small pieces and washed with 25mM triethylammonium bicarbonate (TEAB) in 75% ACN before being dehydrated with 100% ACN and then vacuum dried. Reduction was performed using 5mM Tris 2-carboxyethyl phosphine hydrochloride (TCEP) in 25mM TEAB buffer at 60°C for 30min. Reduced samples were then alkylated with 10mM methyl methanethiosulfonate (MMTS) in 25mM TEAB buffer at room temperature for 45min. The gel pieces were then alternately washed in 25mM TEAB buffer and 25mM TEAB/75% ACN to remove excess TCEP and MMTS. The gel pieces were again dehydrated and dried. In-gel digestion was carried out overnight at 37°C in 25mM TEAB buffer containing 10ng/ml sequencing-grade modified trypsin (Promega Corporation, Madison, WI. USA). Tryptic peptides derived from the supernatant fractions (Nx-S, Hx48-S, Hx72-S and Rx-S) and pellet fractions (Nx-P, Hx48-P, Hx72-P and Rx-P) were labeled with isobars 113, 114, 115, 116, 117, 118, 119 and 121 (Supplementary Table S1). The iTRAQ-labeled peptides were pulled-down together, desalted using Sep-Pak Vac C18 cartridges (Waters, Milford, MA) and dried by vacuum-centrifugation.

ERLIC fractionation and LC-MS/MS analysis

iTRAQ-labeled peptides were dissolved in 100µl sample loading buffer (10mM ammonium acetate in 85% ACN and 1% formic acid) before being fractionated using Electrostatic Repulsion-Hydrophilic Interaction Chromatography (ERLIC). PolyWAX LP™ 20 columns (4.6 × 200mm, 5µm particle size, 300Å

pore size) (PolyLC, Columbia, MD, USA) were used on a 21 Prominence™ HPLC unit (Shimadzu, Kyoto, Japan) for fractionation, during which the flow rate was maintained at 1ml/min. The gradient used for separation comprised 100% buffer A (10mM ammonium acetate in 85% ACN and 0.1% acetic acid) for 5min, 0-28% buffer B (30% ACN and 0.1% formic acid) for 40min, then 28-100% buffer B for 5min, followed by 100% buffer B for 10min. The collected 52 fractions were combined in to 28 fractions according to their chromatogram and then concentrated to dryness using vacuum centrifugation. The ERLIC-fractionated, labeled peptides were reconstituted in 0.1% formic acid for LC-MS/MS analysis using a Q-STAR Elite mass spectrometer coupled with online nano-flow Eksigent HPLC system (Applied Biosystems, MDS-Sciex, Foster City, CA). Nano-bored C18 columns with a picofrit nanospray tip (75µm ID×15cm, 5µm particles) (New Objectives, Wubrun, MA) were used for peptide separation. The entire analysis was carried out at constant flow rate of 300nl/min. The LC-MS/MS analysis was performed in triplicate by injecting the samples three times. All MS data were acquired in positive ion mode with a mass range of 300-2000m/z. Peptides with charge of +2 to +4 were selected for MS/MS and the three most abundant peptide ions above a 5 count threshold were dynamically excluded for 30s with 30mDa mass tolerance. Smart information-dependent acquisition (IDA) was activated with automatic collision energy and MS/MS accumulation. The fragment intensity multiplier was set at 20 and maximum accumulation time was set at 2s.

Mass spectrometric data analysis and bioinformatics

Acquisition of all mass spectrometric data was performed using Analyst QS 2.0 software (Applied Biosystems/MDS SCIEX). Protein Pilot 3 Software (Applied Biosystems, Foster City, CA) was used for the identification and quantification of proteins. The Paragon and ProGroup algorithms were used for peptide identification and isoform-specific quantification during ProteinPilot search. The defined parameters used for the search were; (i) Sample Type, iTRAQ 8-plex (Peptide Labeled); (ii) Cysteine alkylation, MMTS; (iii) Digestion, Trypsin; (iv) Instrument, QSTAR Elite ESI; (v) Special factors, None; (vi) Species, None; (vii) Specify Processing, Quantities; (viii) ID Focus, biological modifications, amino acid substitutions; (ix) Database, The UniProt Knowledgebase (UniProtKB) human protein database (downloaded 12 March 2010: 95,624 sequences and 36,307,192 residues); (x) Search effort, thorough. Other search parameters including precursor and fragment mass tolerance were set at 0.2Da and maximum miscleavage was set at 2. The UniProtKB database and its reversed sequence were combined and used for the searches, and the reverse sequence was used for estimation of false discovery rate (FDR). The peptide for quantification was automatically selected by ProGroup algorithm with criteria; a) the peptide was suitable for quantitation (iTRAQ reporter area >0); b) the peptide was identified with good confidence; 3) the peptide was not shared with another protein that had been identified with higher confidence. The resulting data set was automatically bias-corrected to eliminate variation due to potential unequal mixing while combining iTRAQ-labeled samples. The UniProtKB database was used for the classification and functional annotation of the proteins. Cluster analysis of the identified proteins was conducted according to their abundance in the chromatin digests using the online bioinformatics tool Gene Pattern (http://genepattern.broadinstitute.org) before hierarchical clustering and Pearson correlation were applied.

Post-proteomic validation by dynamic SRM quantification

Chromatins were extracted from the four different hypoxic A431 cells and digested with DNase I as described in the previous section. Digests from three biological replicates were pooled together and used

for shortlisted proteins quantitation by selected reaction monitoring (SRM). 50µg of protein from each condition was taken for in-gel digestion. TSQ vantage triple stage quadrupole mass spectrometer coupled with EASY-nLC™ 1000 nanoflow UHPLC system (Thermo Scientific, MA, USA) was used for the SRM based quantification of tryptic peptides. Peptides and their respective transitions of the targeted proteins were selected according to their intensities from our existing human chromatome data sets by using an in-house algorithm. Tryptic peptides were separated in an Acclaim® PepMap RSLC C18 column (75µm×15cm; nanoViper C18, 2µm, 100Å) fitted with a Acclaim® PepMap100 tap column (75µm×2cm; nanoViper C18, 3µm, 100Å) (Thermo Scientific, MA, USA) by 60min gradient of mobile phase A (0.1% formic acid in water) and mobile phase B (0.1% formic acid in acetonitrile) [45min of 3–30% B; followed by 9min of 30–50% B and 1min of 50–60%; maintained at 60% B for 2 min; finally requilibrated at 3% B for 8min]. Machine parameters were set at optimum including electrospray voltage of 1500V, capillary temperature of 250°C, collision gas pressure of 1mTorr, mass window of 0.7FWHM (full width at half maximum) and scan time of 50ms for the SRM experiment. Retention time of the selected peptide was picked for the 60min full scan data. Dynamic SRM with 5min time window was used for quantification and performed in triplets. Data processing and quantitative analysis were performed using Thermo Pinpoint 1.2.0 software (Thermo Scientific, MA, USA).

Western blot analysis

Equal amounts of protein from each sample were resolved in 10% acrylamide gels and transferred onto nitrocellulose membranes. Immunoblotting was performed using anti-protein antibodies together with the ECL system for detection (Invitrogen, USA).

Flow-cytometry

Cells were washed with ice-cold PBS and fixed in ethanol at -20ºC for 24h. The fixed cells were then stained with 0.5mg/ml propidium iodide for 15min at 37°C. DNA content was measured using a FACSCalibur™ flow cytometer and data were analyzed using CELLQUEST software (BD Biosciences, CA, USA).

HP1BP3 knockdown

HP1BP3 knockdown in A431 and U2OS cells were achieved using shRNA-1 [#RHS4430-101127970] (RNA intro GIPZ Lentiviral shRNAmir Starter Kit, Thermo Scientific Open Biosystems, CA, USA). The pGIPZ clones were grown at 37ºC in low-salt 2X LB broth containing 100µg/ml ampicillin before plasmid extraction was carried out using kits from Axygen, CA, USA. A431 cells were transfected with GIPZ Lentiviral shRNAmir (either HP1BP3-specific or non-silencing control) using the TurboFect Transfection Reagent (Thermo Scientific, CA, USA). Transfected cells were incubated in DMEM containing 10% FBS at 37ºC, 5% CO_2 for 48h. Transgene expression was determined by detection of GFP expression. After 48h, the transfected A431 cells were trypsinized and grown in DMEM containing 2µg/ml puromycin and 10% FBS for a period of 15d to select for stable transfectants. After 15d, each colony was cultured separately and the efficiency of HP1BP3 knock-down was determined by Western blot using an anti-HP1BP3 antibody. The colony that exhibited the most efficient HP1BP3 inhibition was used for subsequent experiments. Another two shRNAs [shRNA-2 (#RHS4430-101127098) and shRNA-3 (#RHS4430-101129419)] were used for HP1BP3 knockdown in A431 cells to confirm the HP1BP3

depletion effects and resulting phenotypes are named HP1BP3Δ(2) and HP1BP3Δ(3).

Chromatin compaction assay

Chromatin samples were extracted from A431 cells, suspended in Micrococcal nuclease (MNase) digestion buffer (50mM tris-Cl pH 7.9, 5mM $CaCl_2$), and then digested with 0-10U MNase at 37ºC for 10min. Digestion was terminated by adding an equal volume of 2X TNESK solution (20mM tris-Cl pH 7.4, 200mM NaCl, 2mM EDTA, 1% SDS, 0.2mg/ml protein kinase K) before incubation overnight at 37ºC. DNA fragments were extracted using phenol-chloroform and DNA content was measured by NanoDrop 2000 UV-Vis Spectrophotometer (Thermo Fisher Scientific, USA). Equal amounts of DNA from each sample were then loaded and resolved on 1% agarose gels.

MTT assay

Cells were grown in normoxia or hypoxia for 48h or 24h hypoxia followed by 24h re-oxygenation before the cultures were supplemented with 0.5mg/ml MTT reagent and incubated at 37ºC for 2h. The culture medium was then aspirated, the formazan crystals dissolved in DMSO, and the optical density of the formazan was measured at 570nm using a micro-plate reader with a reference wavelength of 630nm (Tecan Magellan™, Männedorf, Switzerland).

Clonogenic assay

A total of 500 cells/well were seeded into 6-well plates in DMEM containing 10% FBS and incubated at 37°C in 5% CO_2 for 12d. The culture medium was then aspirated and the cells were washed, fixed with 95% ethanol, and stained with 5% crystal violet. Excess crystal violet was removed by extensive washing and the plate was air-dried overnight at room temperature. The number of colonies formed per well was counted and crystal violet was extracted using 0.5% triton X-100 for colorimetric quantification.

Cell adhesion assay

Cells were grown in normoxia or hypoxia for 48h or 24h hypoxia followed by 24h re-oxygenation, and 24-well plates were coated with 2µg/ml collagen, fibronectin or laminin overnight at 4ºC before addition of 2×10^5 cells/well and incubation in DMEM at 37ºC for 1h. The medium was then removed and the non-adherent cells released by washing with PBS. The adherent cells were fixed with 95% ethanol, stained with 0.5% crystal violet solution, and the excess dye removed by washing before the plates were air-dried overnight at room temperature. Crystal violet was extracted in 0.8ml 0.5% triton X-100 and colorimetrically quantified at 595nm using a microplate reader (Tecan Magellan™, Männedorf, Switzerland).

Scratch-wound assay

Cells were grown to ~100% confluence in 6-well plates and a scratch was made in the middle of the well using a sterile 10µl pipette tip. Then the cells were washed and fresh serum-free medium was added prior to incubation at 37ºC in hypoxia/normoxia for 48h. Images of the scratch area were captured both pre-incubation and after culture in hypoxia/normoxia for 48h. In some experiments, additional images of the

scratch area were captured at 6h and 24h during re-oxygenation. Images were taken by using Nikon Eclipse TE2000-U microscope.

Trans-well assay

Cells were grown in normoxia or hypoxia for 48h or 24h hypoxia followed by 24h re-oxygenation and a total of 4×10^4 cells/well in 100µl serum-free DMEM were seeded into in the upper chambers of a 24-well trans-well plate (8µm pore with polycarbonate filter insert; Costar®, Corning, USA) and the lower chambers were filled with 600µl DMEM containing 2.5% FBS. The plate was incubated at 37ºC in 5% CO_2 for 48h before non-migrated cells (upper surface of the membrane) were removed by wiping with a cotton swab. Migrated cells (lower surface of the membrane) were fixed and stained with 0.5% crystal violet. Excess dye was removed by washing and the membrane was imaged by using Nikon Eclipse TE2000-U microscope. Crystal violet was extracted in 0.5% Triton-X100 solution and used for colorimetric quantification.

Radiation-resistance and chemo-resistance assays

A total of 2×10^5 cells/well were seeded into a 6-well plate and incubated at 37°C for 24h. The culture medium was then replaced with fresh serum-free medium and the cells were treated with 10Gy radiation using a BIOBEAM 2000 gamma irradiation device (Gamma-Service Medical GmbH, Leipzing, Germany). After 24h, the viability of the radiation-treated cells was determined by MTT assay. For chemo-resistance assays, cells were seeded at a density of 1×10^4 cells/well into a 96-well plate and incubated overnight at 37°C before being treated with 0-1600ng/ml doxorubicin for 24h before cell viability was determined by MTT assay.

Sphere formation/self-renewal assay

Cells were grown in normoxia or hypoxia for 48h (or 24h hypoxia followed by 24h re-oxygenation) and then cultured in suspension in DMEM/F12 (1:1) medium supplemented with B27, 20ng/ml epidermal growth factor, 10ng/ml fibroblast growth factor and pen-strep. Cells were seeded into ultra-low attachment flat bottom 24-well plates (Costar®, Corning, USA) at a density of specified number of cells/well and then incubated at 37ºC, 5% CO_2 for 10d. After incubation, the number of tumor spheres formed was counted and images were captured using a Nikon Eclipse TE2000-U microscope.

Xenograft tumor model

Male NCr nude mice (CrTac: NCr-Foxn1nu, Homozygous; InVivos Pte Ltd, Singapore) aged 4-5 weeks and weighing 16-22g each were used for all *in vivo* experiments. Mice were cage-acclimated for 3d in a temperature-controlled environment (24±3ºC) on an alternating 12h light/dark cycle with food and water supplied *ad libitum*. All animal protocols were approved by the Nanyang Technological University Institutional Animal Care and Use Committee. HP1BP3-depleted A431 cells (or mock-depleted control cells) were cultured for 48h, trypsinised, and suspended in sterile PBS for subcutaneous injection of 1×10^6 viable cells into the right flank of each animal (n=6 mice per group). The tumors were grown for 4 weeks

before all mice were euthanized using isoflurane and the tumors were surgically excised for further analysis.

Results and discussion

In-vitro tumor model

Tumor progression is driven by selective pressure on cancer cells applied by the hypoxic conditions in the tumor microenvironment, leading to the clonal evolution of many different types of cancer cells in individual patients. Recent research has uncovered many of the oncogenes and tumor suppressor genes that influence tumor development, but variation in cancer cell types means that it is an extremely challenging task to compile an exhaustive list of all the aberrant molecular events that can promote tumor formation and dissemination. In contrast, hypoxia appears to be a common driver of cancer cell evolution, since gas diffusion cannot supply solid tumors with sufficient oxygen as they progressively increase in size (Figure 1). We therefore hypothesized that hypoxia-sensitive pathways that drive tumor progression to malignant cancer represent promising drug targets for effective cancer treatments.

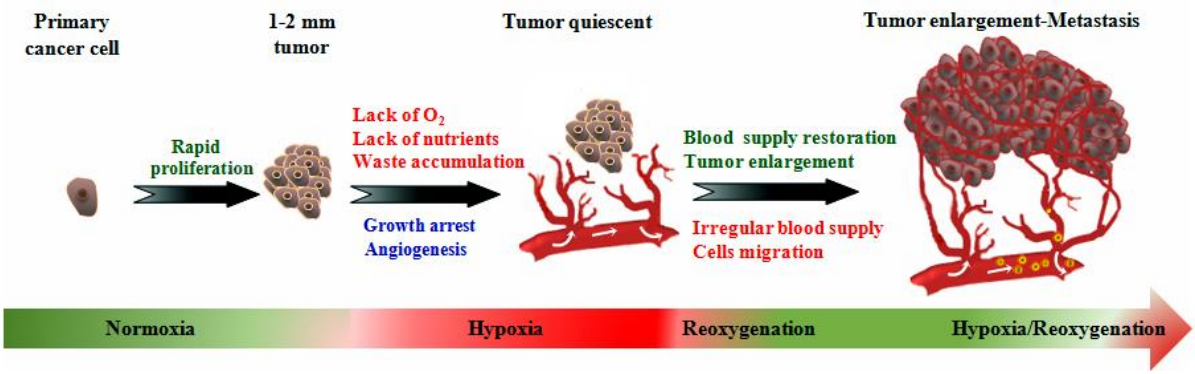

Figure 1: Tumor development and evolution under hypoxic conditions. Cancer starts as a single cell that acquires genetic mutations which promote rapid, uncontrolled growth. When the tumor reaches 1-2mm in diameter, oxygen and nutrient supply by diffusion from nearby blood vessels is insufficient to maintain cancer cell growth. In order to sustain growth and survival under these low-oxygen 'hypoxic' conditions, the cancer cells modify their genome and epigenome via clonal evolution to generate a diversity of cancer cells with distinct properties. At this late stage, cancer cells may spread to other parts of the body and become resistant to both radio- and chemotherapy.

The effects of hypoxia on tumor biology include promotion of cancer cell proliferation, increased migration/invasive behavior, acquisition of stem cell characteristics, and selection of traits that favor survival during hypoxia/re-oxygenation stress(16, 17). Given this central role of hypoxia in both tumor progression and cancer cell development of therapy-resistant properties, we sought to exploit our *in vitro* model of cancer development to conduct a quantitative proteomic analysis of tumor biology under conditions of variable hypoxia stress. To do this, we first cultured cancer cells under normal oxygen conditions (tumor size <2mm) or subjected these cells to hypoxia/re-oxygenation of variable duration (tumor size >2mm) in order to simulate the tumor microenvironment during clonal evolution(18, 19). Using this model, our previous studies of the cancer cell secretome(18) and cellular proteome(19) have already uncovered novel effects of hypoxia on cancer progression. In the current report, we extended our

investigations to assess the influence of low-oxygen conditions on chromatome dynamics in the developing tumor.

Mass spectrometric identification and quantification of the chromatin-associated proteome

In order to study changes in the composition of the chromatin-associated proteome induced by hypoxia and re-oxygenation stress, we cultured A431 cancer cells under conditions of normoxia (Nx), hypoxia (Hx), or hypoxia followed by re-oxygenation (Rx). Chromatin was extracted from the cancer cells and then partially digested with DNase I to extract the euchromatin binding proteins (leaving behind the heterochromatin fraction and matrix-associated proteins in the pellet). Successful fractionation was confirmed by Western blot analysis that indicated high concentrations of GAPDH only in the cytosolic fraction, while high levels of chromatin protein histone H4 were detected only in the chromatin fraction (Figure S1a). Chromatin digests from three biological replicates were pooled and chromatin-associated proteins were then subjected to tryptic digestion and the resultant peptides were labeled with iTRAQ reagent. The labeled peptides were subsequently separated by ERLIC fractionation and then analyzed using an HPLC-coupled QqTOF instrument for identification. ProteinPilot v.3 software was used to compare the mass spectrometric spectra of the peptides against the UniProtKB human protein database. Using this approach, we acquired 1.79×10^5 MS/MS spectra from a total of 84 LC-MS/MS runs (n=3 technical replicates). The distribution of physiochemical properties of the identified proteins indicated a diverse range of molecules within the fractionated samples. Using ProteinPilot searches, we identified a total of 1828 proteins at a level of >99% confidence, with an unused score >2 and false discovery rate (FDR) <1%. Identified proteins that included at least two unique peptides (95% confidence) were then shortlisted for further analysis (1446 proteins total) and were classified according to their subcellular localization as reported in the Uniprot and Nextprot databases. These analysis revealed that the majority of the identified proteins were located in the nucleus (47%) or had no specified subcellular localization (21%) (Supplemental Figure S1c). We then further classified the proteins according to their annotated biological functions and observed that majority were mediators of nuclear processes including regulation of transcription (14%), chromatin organization (8%), DNA repair and replication (4%), mRNA processing (8%), rRNA processing (3%), nuclear transport (3%), cell cycling (2%), ribosome biogenesis (1%), and other miscellaneous chromatin-dependent events (4%) (Supplemental Figure S1d).

In this iTRAQ-based proteomic analysis, we used the supernatant fraction of cells cultured under normoxia for 48h as the denominator for relative quantification of the different samples (with iTRAQ ratio cutoff values of 1.25 and 0.75 for fold-change in protein abundance). Using this approach, we detected 484 proteins that were up-regulated and 506 proteins that were down-regulated in the different fractions of the chromatin digests. We shortlisted 819 of these modulated proteins for further analysis based on the detection of a significant difference in iTRAQ reporter ratio ($p<0.05$) for at least one of the chromatin digests (Table 1). The shortlisted proteins were then clustered according to their relative abundance in the chromatin digests of cells subjected to normoxia, hypoxia, or re-oxygenation protocols. Orthogonal SRM based quantitative proteomic strategy was used for post-proteomic validation using 15 protein candidates. At list 2 peptides for each protein and 3-5 strongest transitions for each peptide (see “SRM Validation of iTRAQ Results (Hypoxia Cancer Progression)” in the supplemental material) were used for SRM quantitation. SRM quantification results (Supplemental Figure S2) showed comparable chromatin binding

topology to the iTRAQ results, indicating the reproducibility and reliability of our chromatome profiling strategy.

Table 1:

Proteins identified in the chromatin digests.

	Number of proteins with significant change in iTRAQ ratio (p-value <0.05)							
Sample*	**Hx48-S**	**Hx72-S**	**Rx-S**	**Nx-P**	**Hx48-P**	**Hx72-P**	**Rx-P**	**Total unique protein****
iTRAQ ratio	**114:113**	**115:113**	**116:113**	**117:113**	**118:113**	**119:113**	**121:113**	
p-value<0.05	271	326	310	494	482	489	474	819
Ratio>1.25	80	100	97	195	187	194	187	484
Ratio<0.75	87	166	78	270	266	273	254	506

***** Ratios are calculated using Nx-S as denominator. Supernatant fractions Nx-S, Hx48-S, Hx72-S and Rx-S and pellet fractions Nx-P, Hx48-P, Hx72-P and Rx-P were obtained by partial DNase I digestion of respective chromatin extracted from normoxic (Nx), 48h hypoxic(Hx48), 72h hypoxic(Hx72) and reoxygenated(Rx) A431 cells.; ******Number of unique proteins with at least one iTRAQ ratio exhibiting significant change ($p<0.05$).

Chromatin organization and transcriptional regulation during hypoxia

The hypoxic tumor microenvironment plays a central role in both local and systemic cancer cell proliferation and contributes to the acquisition of radio- and chemo-resistant properties(20). Low-oxygen conditions are also known to critically influence numerous chromatin-dependent biological events such including transcription(21), replication(22), DNA repair(23), genomic rearrangement(24), and genome amplification(25). Since dynamic changes in the composition and topology of the chromatin-associated proteome critically regulate these key cellular functions in response to changing environmental conditions, it is likely that a better understanding of how chromatome architecture is modified during hypoxia will shed light on numerous important aspects of tumor biology. In the current quantitative proteomic study, we identified a total of 114 proteins involved in chromatin organization and transcriptional regulation that were subject to modulation by changing environmental oxygen levels. Figure 2, Supplemental Figures S3a-S3d and S4a-S4f show the differential release of these proteins by partial DNase I digestion of the chromatin samples obtained from the cancer cells cultured under different conditions. Further analysis of these proteomic data enabled the identification of 7 distinct protein clusters (a-g) that shared similar chromatin association topology under specific oxygenation conditions and displayed comparable patterns of release by DNase I digestion (Figure 2). Proteins in cluster a were enriched in chromatin extracts from cells cultured under normoxic conditions, but displayed reduced chromatin association during hypoxia. These molecules included proteins DEK and INO80, as well as the condensin complex subunits SMC2, SMC4, NCAPD2 and NCAPG (Figures 2 and supplemental Figures S3a-S3d). Similarly, cluster c proteins incorporated the chromatin organizing proteins CHAF1B, DNMT1, UHRF1 and CHD4, which were abundant only in the supernatant fraction of normoxic samples (Supplemental Figures S3b and S3d), indicating that hypoxia stress substantially reduced their binding to chromatin. Since chromatin organizing proteins and molecular platforms such as the condensin complex are closely associated with cell cycle regulation, it is possible that reduced chromatin binding by proteins in clusters a and c could be attributed to cell cycle disruption due to hypoxia stress(26, 27). Consistent with these proteomic data, our cell cycle analysis of cancer cells that had

been subjected to hypoxia revealed a corresponding cell cycle arrest in G_0-G_1 phase (Supplemental Figures S5b-S5c).

Our DNase I digestion data indicated that key epigenetic regulators including PRMT1, TOX4 and the NuRD complex components HDAC2, MBD2, MTA1 and MTA2, were rapidly released by partial digestion and were relatively abundant in the re-oxygenated supernatant samples (cluster d; Supplemental Figures S3b-S3d). Recent findings suggest that HDACs can regulate apoptosis and mediate expression of VEGF and HIF-1α in hypoxia-stressed cells(28), and MTA family proteins are reported to be pro-metastatic molecules that are overexpressed in a wide range of cancers(29). Protein arginine methyltransferases (PRMTs) have also been identified as exerting critical roles in cell proliferation and modulation of the tumor microenvironment(30), hence increased euchromatin binding of HDACs, MTA proteins and PRMTs during re-oxygenation would be expected to alter gene expression and potentially enhance oncogenesis/metastasis in developing cancer cells. Cluster d proteins that were enriched in the re-oxygenated supernatant fraction also included numerous transcription factors (CCAR1, KHSRP, GTF3C3, GTF3C5, ILF2 and ILF3) consistent with euchromatin binding of these proteins and modification of gene expression during re-oxygenation.

Proteins in ‘cluster e’ and ‘cluster g’ were enriched in the supernatant fraction of chromatin extracted from cells that had been subjected to hypoxia for 48h, but were depleted from digests of cells that had been subjected to longer periods of hypoxia. These proteins included the transcriptional regulator MECP2, polymerase POLR2G, and multiple transcription factors (GCFC, GTF3C4, TAF2, TAF4 and TAF9) (Supplemental Figures S3d and S4e). Hypoxia-induced binding of MECP2 in the hyper-methylated CpG island of euchromatin mediates silencing of tumor suppressor genes and increases cancer cell survival during hypoxia stress(31), and reduced chromatin binding of TAF molecules is associated with activation of the p53-induced pathway of apoptosis after prolonged hypoxia(32). In contrast, the proteins grouped in cluster f (including JUND and SMAD3) (Figure 2 and Supplemental Figures S4a-S4b) were instead enriched in the chromatin supernatants of cells cultured under hypoxia for 72h, suggesting increased euchromatin binding only after prolonged oxygen deprivation, and indicating that these proteins might contribute to oncogene activation in developing tumors(33, 34).

Quantitative proteomic profiling revealed that cluster b proteins, including the transcriptional regulators NAT10, CIRH1A and NOC2L, and chromatin organizing proteins HP1BP3 and KDM5B, remained unreleased by DNase I digestion and were detected at high levels in hypoxic chromatin pellets compared with other digests (Figures 2 and Supplemental Figure S3a). These data indicated increased binding of cluster b proteins to heterochromatin in response to hypoxia stress, consistent with a role for these molecules in the repression of tumor suppressor genes during malignant progression(35, 36). In

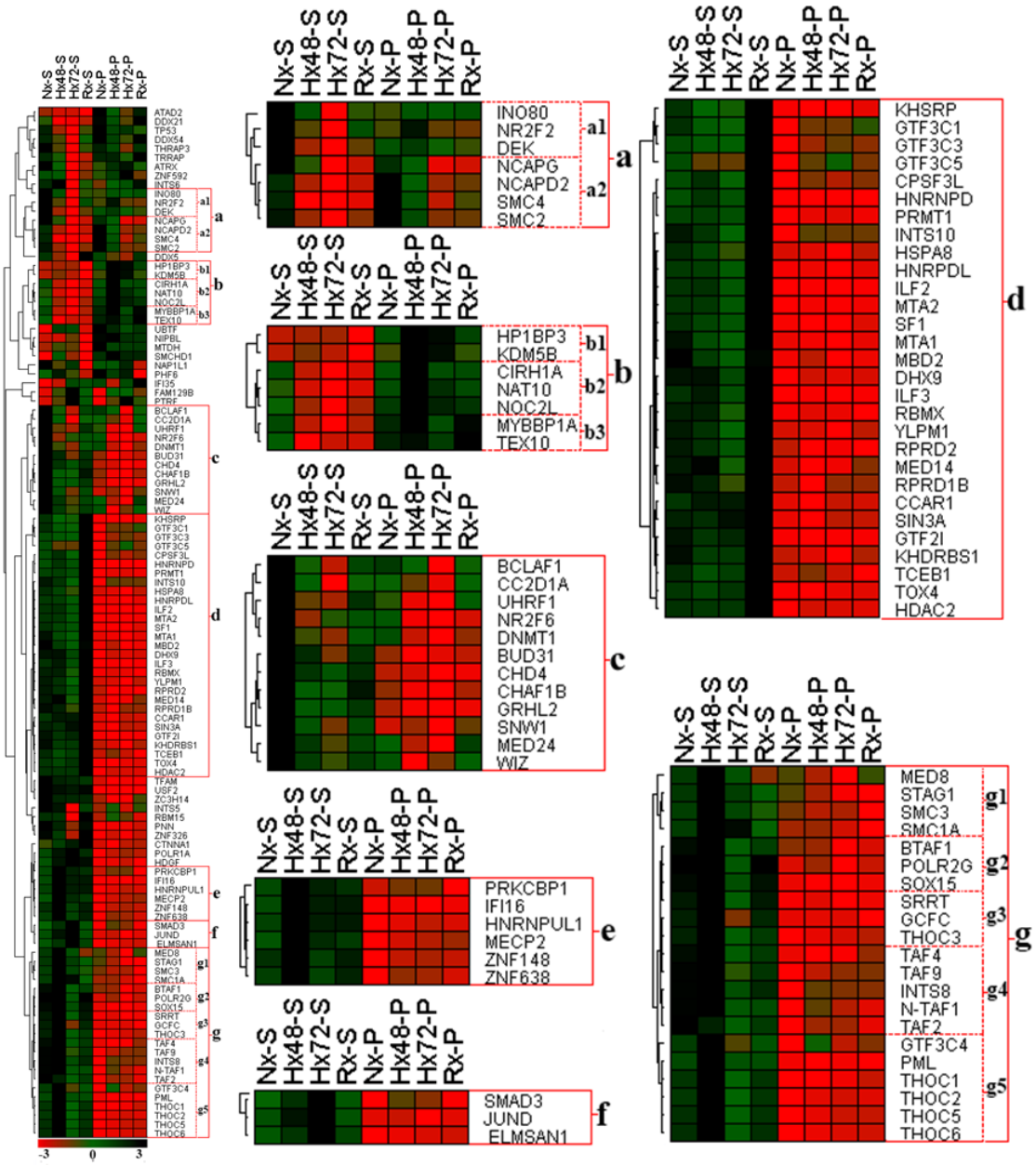

Figure 2: Hierarchical clustering of chromatin organizer proteins and transcriptional regulators. A431 cancer cells were cultured under variable conditions of normoxia (Nx), 48h hypoxia (Hx48), 72h hypoxia (Hx72), or 48h hypoxia followed by 24h re-oxygenation (Rx). Chromatin was then extracted from the cells and subjected to partial DNase I digestion to release euchromatin-binding proteins into the supernatant (suffix S) and leave heterochromatin-bound proteins behind in the undigested pellet (suffix P). Cluster analysis of these data identified a group of proteins that were enriched in Nx samples (cluster a) either in the supernatant fraction (Nx-S; cluster a1) or in the pellet fraction (Nx-P; cluster a2). Cluster b proteins were instead associated with hypoxia and were enriched in both the Hx48 and Hx72 pellet samples (cluster b1), or in the Hx48-P fraction only (cluster b2), or in both the Hx48-P and Rx-P fractions (cluster b3). Other proteins were detected at high concentrations only in a single sample fraction, including cluster c (Nx-S), cluster d (Rx-S), cluster e (Hx48-S) and cluster f (Hx72-S). Finally, proteins in clusters g1, g3 and g5 were comparatively enriched in the Hx48-S fraction, whereas clusters g2 and g4 displayed high abundance in both the Nx-S and Hx48-P fractions.

agreement with our proteomic data, other investigators have recently reported a role for KDM5B in regulating the expression of E2f genes via re-modelling of heterochromatin during cell cycle progression(37), and our Western blot analysis confirmed that HP1BP3 binding to chromatin was increased by hypoxia stress (Supplemental Figures S6a-S6b). Indeed, we have previously demonstrated that HP1BP3 plays an important role in the maintenance of heterochromatin integrity, and that depletion of HP1BP3 increases the MNase sensitivity of chromatin samples(38). Accordingly, our MNase digestion experiments confirmed that hypoxia increased chromatin resistance to nuclease activity, suggesting that these samples contained increased proportions of heterochromatin compaction (Figure 3). Taken together, our proteomic and biological data were consistent with a role for HP1BP3-mediated chromatin condensation in hypoxia-induced gene modulation in tumorigenesis.

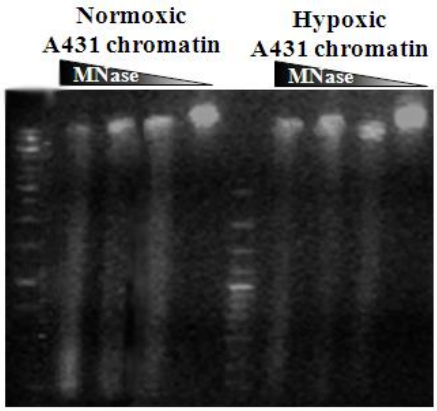

Figure 3: Hypoxia is associated with increased chromatin resistance to nuclease digestion. Agarose gel separation of MNase-digested chromatin obtained from A431 cancer cells subjected to either normoxia or hypoxia. Data suggest increased proportions of heterochromatin compaction in cells cultured under low-oxygen conditions.

HP1BP3 is a novel regulator of tumor biology during hypoxia

Since HP1BP3 is directly involved in heterochromatin organization and regulation of gene transcription(38), so we next tested if HP1BP3 mediates global heterochromatinization during hypoxia stress by depleting HP1BP3 in A431 cells with shRNAs (Supplemental Figures S7a-S7c), and observing the effects of HP1BP3 deficiency on tumor progression in low-oxygen conditions. HP1BP3 depletion effects were reconfirmed by repeating few important experiments with different shRNAs.

Having previously established that hypoxia reduces cell viability and induces cell cycle arrest at G_0-G_1 phase (Supplemental Figures S5a-S5c), taken together with our previous report that HP1BP3 promotes G_1/S transition(38), we next sought to determine the effects of HP1BP3 knock-down on cancer cell growth *in vitro*. Our MTT assays and clonogenicity experiments indicated that HP1BP3-depleted A431 cells were more proliferative relative to their mock-depleted counterparts during normal cell culture condition (Figures 4a and 4c-4d and Supplemental Figures S8a-S8c) that suggested a role for HP1BP3-induced heterochromatinization in G_0-G_1 arrest during hypoxia. HP1BP3-depleted cells also displayed loss of clonogenicity during hypoxia stress, but formed larger colonies than those generated by mock-depleted

cells (Figures 4e-4f). These data indicated that depletion of HP1BP3 reduced cell viability during hypoxia but simultaneously increased the proliferation of the surviving cells. Previous experimental data have indicated that hypoxia-induced cell cycle arrest in G_0-G_1 phase can increase survival by suppressing the p53-induced pathway of apoptosis(39). Indeed, our Western blot analysis revealed that p53 expression levels were increased by ~1.8 fold in HP1BP3-depleted A431 cells (Supplemental Figures S9a-b), and our proteomic data indicated that the extent of p53 association with chromatin was reduced during hypoxia stress (Supplemental Figure S4f). We therefore propose that HP1BP3-mediated heterochromatinization induces transcriptional reprogramming as well as cell cycle arrest in G_0-G_1 phase to reduce apoptotic death and promote cancer cell survival.

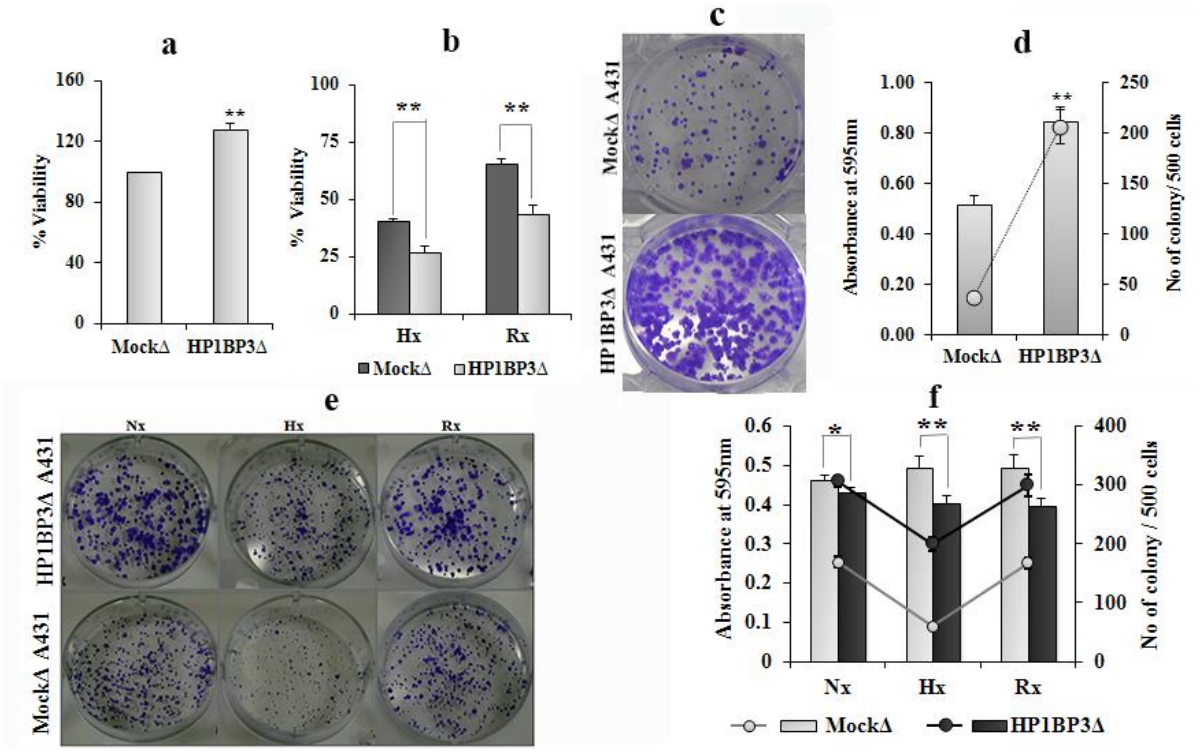

Figure 4: HP1BP3 depletion differentially modulates cancer cell viability and clonogenicity. Viability of HP1BP3-depleted A431 cells as assessed by MTT assay after 24h culture under normoxia (a), or the same cells subjected to 48h hypoxia or 24h hypoxia/24h re-oxygenation (b), with survival expressed relative to the viability of mock-depleted control cells. Representative images and quantification of crystal violet staining in HP1BP3-depleted A431 cells and mock-depleted control cells after 10d culture in normoxic conditions (c and d) or the same cells subjected to 48h normoxia, 48h hypoxia, or 24h hypoxia/24h re-oxygenation prior to culture (e and f). Each experiment was performed in triplets (*P<0.05, **P<0.005).

Regulatory role of HP1BP3 in ECM adhesion and cell migration

In vivo, tumor cells are surrounded by a complex extracellular matrix (ECM) that exerts a critical influence on tumor cell morphology, proliferation, survival, migration, invasion and differentiation(40-42). We have previously shown that hypoxia stress alters cancer cell adhesion and metastatic potential by

changing the expression of key ECM proteins(18, 19). In order to assess the role played by HP1BP3 in cancer cell motility, we investigated the impact of HP1BP3 knock-down on the efficiency of cell adhesion to matrices including collagen type I, fibronectin and laminin. Depletion of HP1BP3 significantly increased cancer cell adhesion to collagen and laminin, whereas binding to fibronectin was markedly reduced (Supplemental Figures S10a-S10b). Conversely, under hypoxia, cancer cell adhesion to collagen and laminin was substantially reduced, whereas binding to fibronectin was enhanced (Figure 5a-c). However, HP1BP3 depletion also has a significant influence on hypoxia induced cancer cell adhesion to different ECM components (Figures 5a-5c). Our previous studies showed depletion of HP1BP3 lead to altere expression levels of adhesion molecules including up-regulation of integrin alfa-6 and beta-4and down-regulation of beta-1isoforms (38) which might be responsible for alternation of the adhesion property of HP1BP3 depleted cells. Thus hypoxia-induced chromatin condensation as mediated by HP1BP3 may instead expression of adhesion molecules including integrin isoforms in cancer cell that critically regulate migratory potential as observed in our previous study(19).

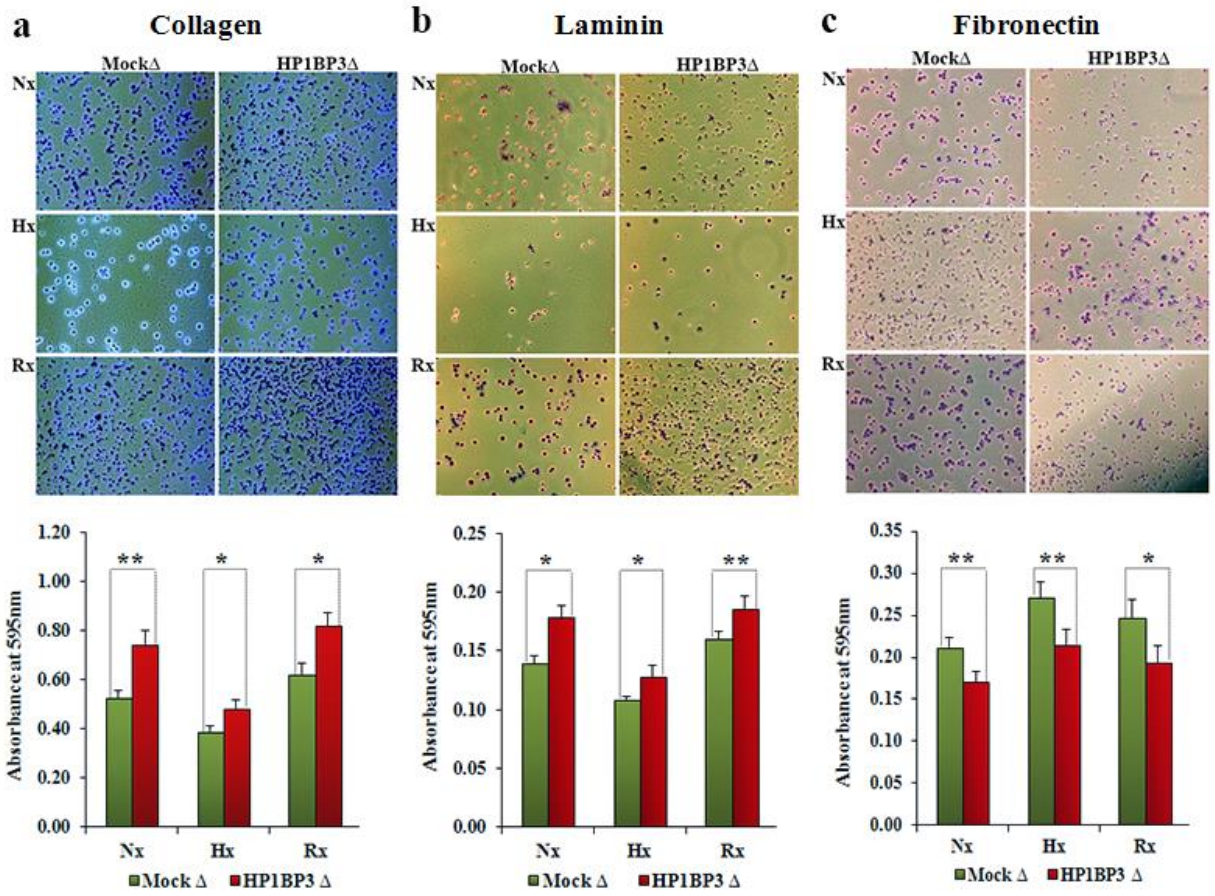

Figure 5: HP1BP3-dependent modulation of cancer cell adhesion during hypoxia. A431 cells were subjected to 48h normoxia (Nx), 48h hypoxia (Hx), or 24h hypoxia followed by 24h re-oxygenation (Rx) and then assessed for adhesion to collagen (a), laminin (b) and fibronectin (c) based matrices. Each experiment was performed at list in triplicate (*P<0.05, **P<0.005).

Hypoxia-induced tumor cell migration and tissue invasion play major roles in the metastasis of cancers(18). We therefore performed wound healing and trans-well assays to investigate the requirement for HP1BP3 in cancer cell migration *in vitro*. These analyses indicated that cancer cell migration was significantly increased following HP1BP3 depletion, and was further augmented by culture under conditions of hypoxia or re-oxygenation (Figures 6a-6d). Since highly migratory and invasive cancer cells are characterized by loss of cell-cell adhesion and increased binding to ECM components(43), our observations suggest that HP1BP3-mediated heterochromatinization can reprogram gene expression to increase cancer cell migration by modifying key interactions with the ECM according to the prevailing oxygen level in the local microenvironment.

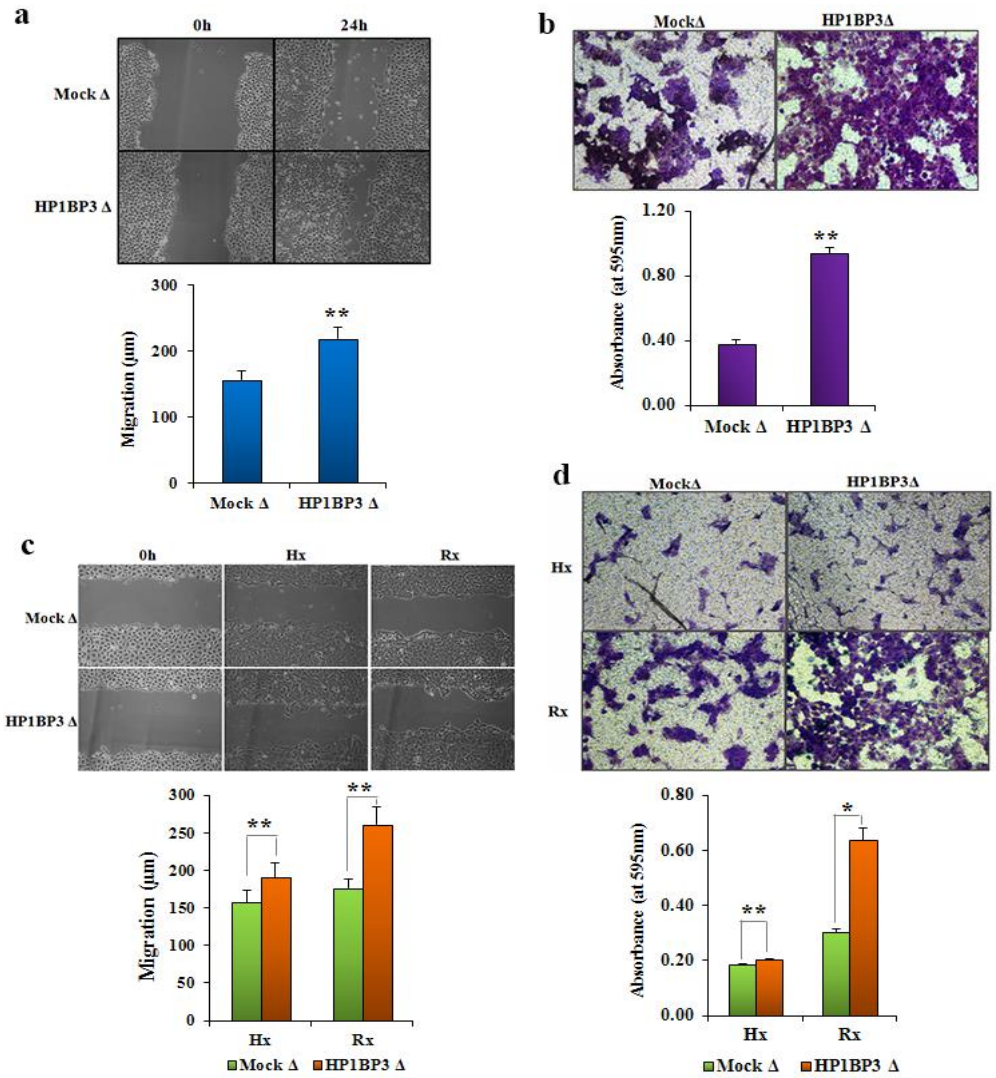

Figure 6: HP1BP3-mediated regulation of cell migration. a: Effect of HP1BP3 depletion on cell migration as assessed by scratch assay (a) or trans-well assay (b) conducted under normoxic conditions, or the same assays conducted with cells that had been subjected to 48h hypoxia or 24h hypoxia/24h re-oxygenation (c and d). Each experiment was performed at list in triplicate (*P<0.05, **P<0.005).

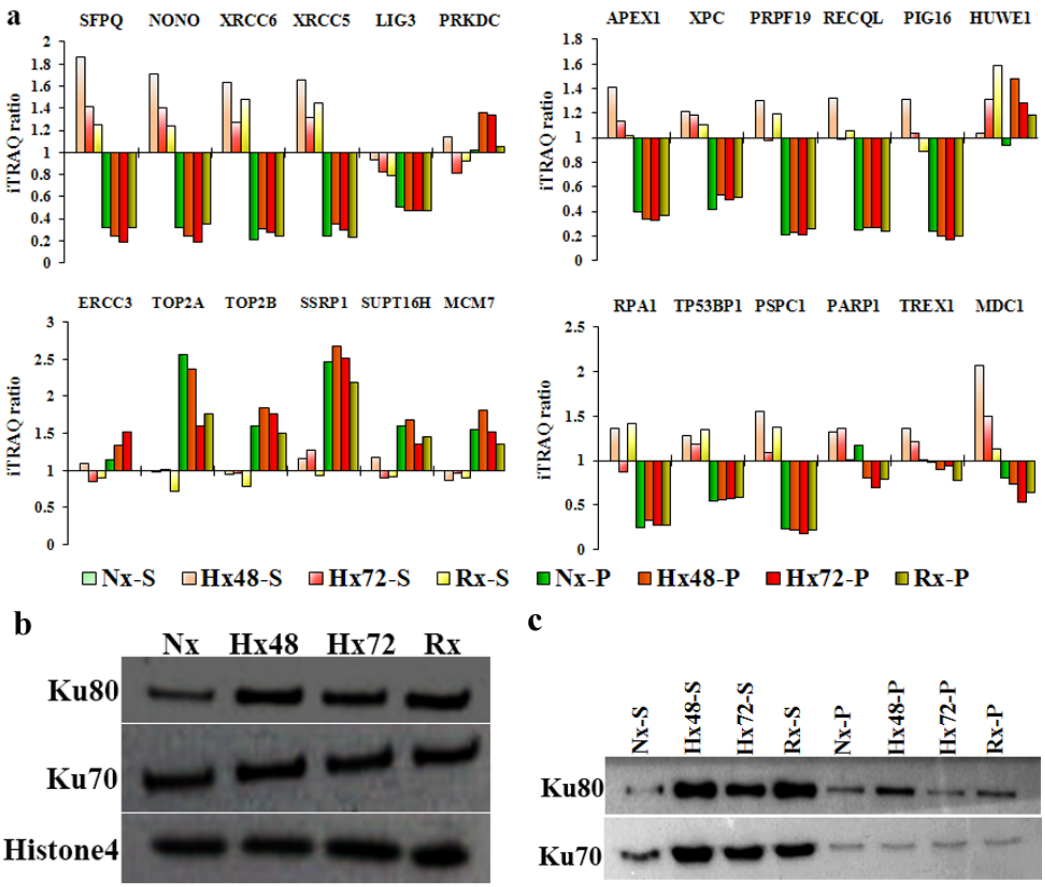

Figure 7: Differential chromatin-association of DNA repair proteins during hypoxia stress. a: iTRAQ ratio indicating the relative abundance of different proteins in the samples. b: Western blot showing the chromatin-association levels of proteins Ku70, Ku80 and histone H4 in samples extracted from A431 cells cultured under normoxic conditions for 48h (Nx), 48h hypoxia (Hx48), 72h hypoxia (Hx72), or 48h hypoxia/24h re-oxygenation (Rx). c: Western blot indicating the quantities of Ku80 and Ku70 proteins obtained by partial DNase I digestion of the chromatin samples (supernatant fraction, suffix S; pellet fraction, suffix P).

Hypoxia and HP1BP3 in radio- and chemo-resistance

Extensive clinical and experimental data have established that hypoxia induces cancer cell resistance to radio- and chemotherapy, as well as promoting genetic instability and metastasis(44-46). While therapeutic use of ionizing radiation and chemotherapeutic agents are known to induce DNA double strand breaks (DSBs) that trigger apoptosis of cancer cells, the effects of hypoxia-induced genetic instability on DNA repair mechanisms in developing tumors are not well understood. Multiple mechanisms can repair DSBs in damaged host cells, including non-homologous end joining (NHEJ) and homologous recombination (HR). Our iTRAQ-based proteomic data and western blot analyses confirmed that the NHEJ-associated proteins XRCC5 and XRCC6 were enriched in the supernatant fractions of chromatin extracted from cells cultured in low-oxygen or re-oxygenation conditions (Hx48-S, Hx72-S and Rx-S), whereas a third NHEJ-associated protein PRKDC was instead identified at high concentrations only in the pellet

fractions of hypoxic chromatin samples (Figures 7a-7e). These data suggested that the NHEJ pathway is active in cancer cells that have been subjected to hypoxia, consistent with our recent report that NHEJ-associated proteins are up-regulated during hypoxia/re-oxygenation of cancer cells and contribute to radio- and chemo-resistance(19). Proteomic profiling also identified hypoxia/re-oxygenation-induced increases in chromatin binding by NHEJ facilitator proteins (MDC1, NONO, and SFPQ) and alternative DSB-associated proteins (APEX1, PIG16, PRPF19, RECQL, XPC, PSPC1, RPA1, and TP53BP1) (Figure7a). DSB repair by homologous recombination (HR) is restricted to the late S and G_2 phases of the cell cycle, whereas NHEJ repair of DSBs can occur throughout interphase(47, 48), and our previous analyses of cell cycle-associated changes in the chromatome suggested that NHEJ repair mechanisms operate throughout interphase but are particularly active during G_1 and G_2(38). Our findings are therefore consistent with the concept that hypoxia induces G_0-G_1 cycle arrest to enhance NHEJ-mediated repair of DSBs and increase cancer cell resistance to radio- and chemo-therapy. In addition to NHEJ-based DNA repair, hypoxia can also influence both the expression and chromatin binding topology of multiple other proteins that confer cancer cells with increased radio- and chemo-resistance. Having already observed that HP1BP3 expression is associated with increased cancer cell viability during hypoxia, we next sought to determine the role of this protein in radio- and chemo-resistance. To do this, we treated HP1BP3-depleted A431 cells (or mock-depleted control cells) with either 10Gy ionizing radiation or doxorubicin for 24h and assessed cell viability by MTT assay. We observed that HP1BP3 depletion increased cancer cell susceptibility to both radiation treatment (viability decreased ~18%; Figure 8a), and doxorubicin exposure (IC_{50} of doxorubicin treatment decreased from 670.2±62ng/ml to 503.2±36ng/ml; Figure 8b). Taken together, our data reveal a novel role for HP1BP3-induced heterochromatinization in genetic reprogramming of cancer cells during hypoxia, leading to the acquisition of radio- and chemo-resistant characteristics.

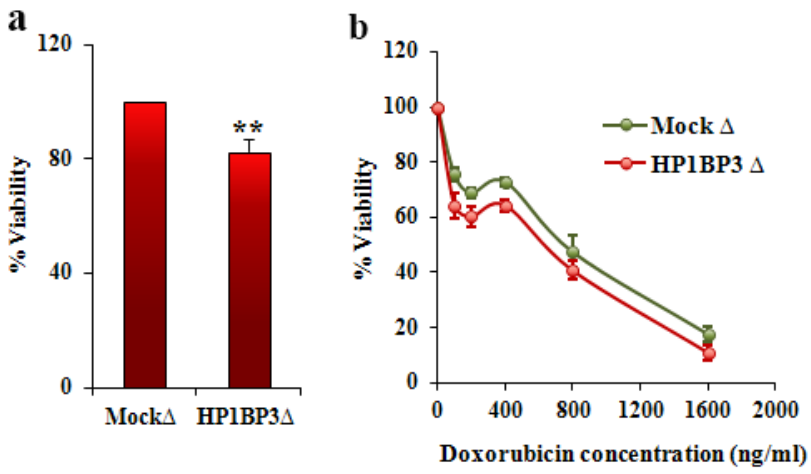

Figure 8: HP1BP3 decreases cancer cell resistance to radio- and chemo-therapy. Viability of HP1BP3-deleted A431 cells as measured by MTT assay after exposure to 10Gy ionizing radiation (a) or after treatment with 0-1600 ng/ml doxorubicin (b) compared with mock-depleted control cells (n=6 experimental replicates,**P<0.005).

Hypoxia and HP1BP3 in self-renewal of cancer stem cells

Cancer stem cells (CSCs) exhibit stem-cell like properties and are thought to play a critical role in the initiation and development of tumors. Previous reports have identified that HIF expression in response to low-oxygen conditions induces changes in gene expression that imbue CSCs with increased capacity for self-renewal and multipotency during cancer progression(49-51). We therefore hypothesized that HP1BP3-induced heterochromatinization and transcriptional reprogramming of cancer cells can promote the generation of CSC-like cells in developing tumors. To do this, we conducted sphere formation assays using different HP1BP3 depleted A431 and U2OS phenotypes in which we observed that over a 10d culture period, HP1BP3-depleted A431 cells generated far smaller tumor spheres (mean diameter 25±5μm) than did their mock-depleted counterparts (mean diameter 82±15μm) (Supplemental Figures S11a-S11c). The number of tumor spheres formed by mock-depleted A431 cells was also ~4-fold higher than that generated by HP1BP3-depleted A431 cells (Supplemental Figure S11b). While other two HP1BP3 depletion A431 phenotypes obtained by using different shRNAs showed comparable results

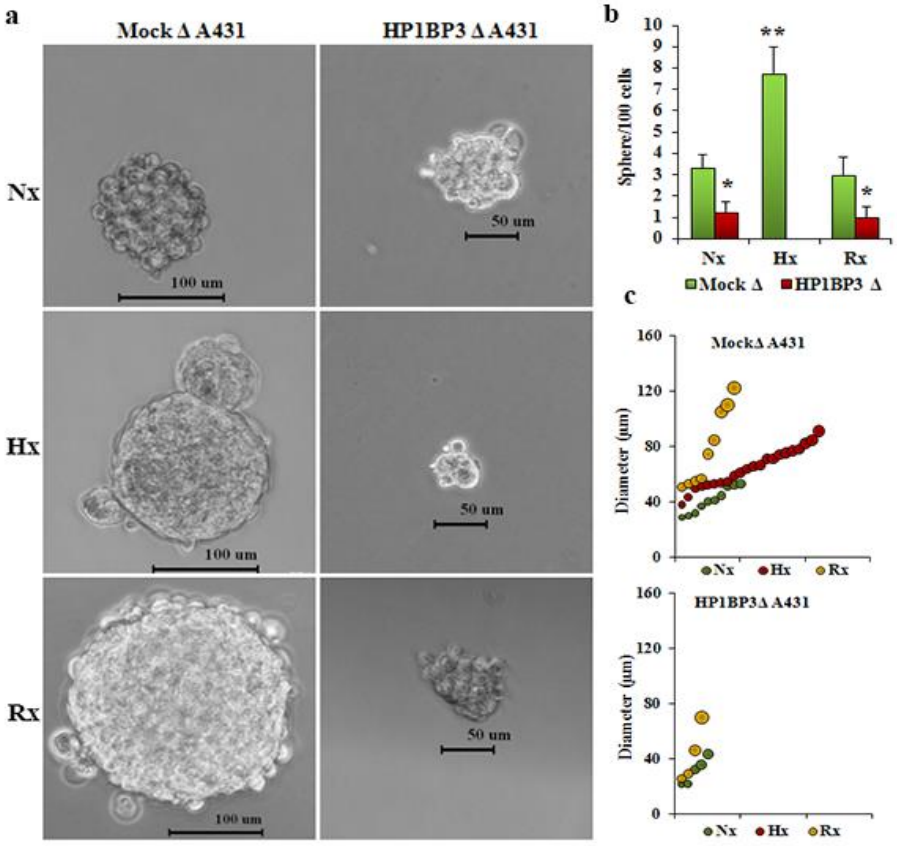

Figure 9: HP1BP3 depletion inhibits cancer cell renewal during hypoxia/re-oxygenation. HP1BP3-depleted A431 cells were cultured for 48h in normoxia (Nx), 48h hypoxia (Hx), or 24h hypoxia/24h re-oxygenation (Rx), and then assessed for tumor sphere formation over 10d of culture (a and b). Size distribution of tumor spheres formed by HP1BP3-depleted A431 cells subjected to the same conditions (c). Each experiment was performed in triplets (*P <0.05, **P<0.005).

(Supplemental Figures S11d-S11f) suggesting their on target effect. While similar effect was observed in U2OS cells upon HP1BP3 depletion (Supplemental Figures S12a-S12c) suggesting HP1BP3 regulates cancer cells Self-renewal property in cell line independent manner. These data were in-line with our hypothesis that HP1BP3-mediated heterochromatinization induces changes in gene expression that regulate the self-renewal potential of CSC-like cancer cells. When we subjected A431 cells to either hypoxia or hypoxia/re-oxygenation prior to commencing the tumor sphere assay, we observed that tumor formation by mock-depleted A431 cells was ~2.5-fold more efficient under hypoxic conditions relative to either normoxia or re-oxygenation conditions (Figure 9). In contrast HP1BP3-depleted cancer cells displayed inefficient tumor sphere formation in normoxia or re-oxygenation conditions, and failed to generate any tumor spheres at all under hypoxic conditions (Figure 9b). Analysis of tumor size distribution further revealed that the average diameter of tumor spheres generated by mock-depleted cancer cells was increased during hypoxia (65±7μm) and re-oxygenation (80±13μm) relative to normoxia (41±5μm) (Figure 9c). In contrast, the average sphere diameter formed by HP1BP3-depleted cells was not significantly altered by the hypoxia/re-oxygenation protocol (34±6μm) relative to normoxia (30±4μm). Effect of HP1BP3 depletion upon tumor sphere formation was further confirmed by using another two different shRNAs (Supplemental Figure S13). Comparable results were also observed in mock and HP1BP3-depleted U2OS cells under similar conditions (Supplemental Figure S14). Taken together, these data suggest that hypoxia-induced acquisition of CSC-like capacity for self-renewal is regulated in a HP1BP3-dependent manner.

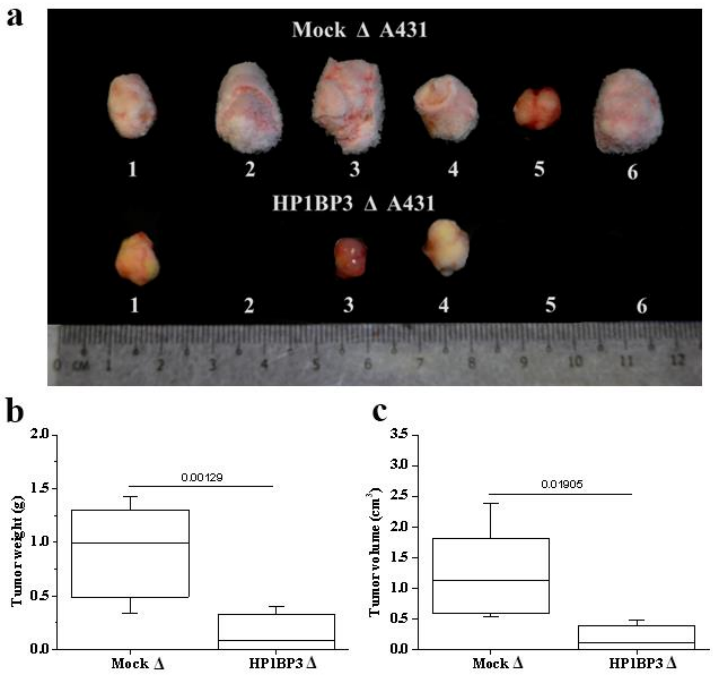

Figure 10: HP1BP3-depleted A431 cells exhibit reduced tumorigenicity *in vivo*. a: Images of tumors formed by HP1BP3-depleted A431 cells *in vivo* compared with mock-depleted control cells. b and c: Mass/size distribution of tumors showing that mock-depleted A431 cells generate larger tumors than HP1BP3-depleted cells (n=6 NCr nude mice per group, p-value <0.05).

Role of HP1BP3 in tumorigenesis

Our cell line-based experiments strongly implicated HP1BP3 in the regulation of multiple biological processes that might contribute to cancer growth and malignancy. We therefore evaluate the role of HP1BP3 in oncogenesis *in vivo* using a xenograft animal model of tumor growth. Using this approach, we observed that mock-depleted A431 cells produced tumors in all six mice that received these cells via *s.c.* injection, whereas HP1BP3-depleted cells produced tumors in only three of six mice injected with these cells. The tumors generated by HP1BP3-depleted cells also displayed significantly reduced size and mass relative to the tumors generated by mock-depleted cells (Figures 10a-10c). Taken together with our cell line-based experiments that suggested a role for HP1BP3 in promoting cancer cell viability, self-renewal, and resistance to therapy, our xenograft tumor data suggest that HP1BP3 depletion is associated with loss of CSC-like properties, leading to reduced tumorigenic potential both *in vitro* and *in vivo*. Our findings are thus consistent with a recent report that disruption of genes which regulate the 'stemness' of CSCs markedly reduces tumorigenic potential(52), and suggest that therapeutic targeting of HP1BP3 may represent a novel approach to treatment in a range of different malignancies.

Conclusion

In this study we used partial DNase I digestion together with an iTRAQ-based quantitative proteomics approach to delineate the chromatin association topology of the proteins that comprise the chromatome, and to establish how these molecules are modulated in cancer cells subjected to low-oxygen conditions. While hypoxia-induced evolution of chromatin biology is known to play a crucial role in oncogenesis, data that describe global changes in the chromatome dynamics which regulate cellular responses to changing environmental conditions are extremely limited. In our study, we identified that the chromatin-binding protein HP1BP3 altered its binding topology in a hypoxia-dependent manner and promoted heterochromatinization in order to modulate gene expression and induce cancer cells to acquire a CSC-like phenotype. Accordingly, depletion of HP1BP3 decreased cancer cell viability, therapy resistance and stemness under hypoxic conditions, leading to decreased tumorigenic potential of these cells both *in vitro* and *in vivo*. These data suggest that targeting of HP1BP3 might provide new therapeutic approaches in a wide range of human cancers.

Supplementary information

Supplementary Figures
Protein Summary-Chromatome (Hypoxia Cancer Progression)
Peptide Summary-Chromatome (Hypoxia Cancer Progression)
SRM validation of iTRAQ results (Hypoxia Cancer Progression**)**

Acknowledgements

This work is in part supported by the Singapore National Research Foundation under its CBRG (NMRC/CBRG/0004/2012) administered by the Singapore Ministry of Health's National Medical Research Council, and the Singapore National Research Foundation under its CRP (NRF2011 NRF-CRP 001-109).

References:

1. Ruan, K., Song, G., and Ouyang, G. (2009) Role of hypoxia in the hallmarks of human cancer. *J Cell Biochem* 107, 1053-1062.

2. Brizel, D. M., Dodge, R. K., Clough, R. W., and Dewhirst, M. W. (1999) Oxygenation of head and neck cancer: changes during radiotherapy and impact on treatment outcome. *Radiother Oncol* 53, 113-117.

3. Nordsmark, M., Overgaard, M., and Overgaard, J. (1996) Pretreatment oxygenation predicts radiation response in advanced squamous cell carcinoma of the head and neck. *Radiothe Oncol* 41, 31-39.

4. Ghattass, K., Assah, R., El-Sabban, M., and Gali-Muhtasib, H. (2013) Targeting hypoxia for sensitization of tumors to radio- and chemotherapy. *Curr Cancer Drug Targets* 13, 670-685.

5. Nguyen, M. P., Lee, S., and Lee, Y. M. (2013) Epigenetic regulation of hypoxia inducible factor in diseases and therapeutics. *Arch Pharm Res* 36, 252-263.

6. Li, P., Zhou, C., Xu, L., and Xiao, H. (2013) Hypoxia enhances stemness of cancer stem cells in Glioblastoma: An in vitro study. *Int J Med Sci* 10, 399-407.

7. Moyer, M. W. (2012) Targeting hypoxia brings breath of fresh air to cancer therapy. *Nat Med* 18, 636-637.

8. Wu, C. Y., Tsai, Y. P., Wu, M. Z., Teng, S. C., and Wu, K. J. (2012) Epigenetic reprogramming and post-transcriptional regulation during the epithelial-mesenchymal transition. *Trends Genet* 28, 454-463.

9. Johnson, A. B., and Barton, M. C. (2007) Hypoxia-induced and stress-specific changes in chromatin structure and function. *Mutat Res* 618, 149-162.

10. Wang, F., Zhang, R., Beischlag, T. V., Muchardt, C., Yaniv, M., and Hankinson, O. (2004) Roles of Brahma and Brahma/SWI2-related gene 1 in hypoxic induction of the erythropoietin gene. *J Biol Chem* 279, 46733-46741.

11. Isaacs, J. T., Antony, L., Dalrymple, S. L., Brennen, W. N., Gerber, S., Hammers, H., Wissing, M., Kachhap, S., Luo, J., Xing, L., Bjork, P., Olsson, A., Bjork, A., and Leanderson, T. (2013) Tasquinimod Is an Allosteric Modulator of HDAC4 survival signaling within the compromised cancer microenvironment. *Cancer Res* 73, 1386-1399.

12. Steinmann, K., Richter, A. M., and Dammann, R. H. (2011) Epigenetic silencing of erythropoietin in human cancers. *Genes Cancer* 2, 65-73.

13. Tsai, Y. P., and Wu, K. J. (2013) Epigenetic regulation of hypoxia-responsive gene expression: focusing on chromatin and DNA modifications. Int. J. Cancer 134, 249-256.

14. Robinson, C. M., Neary, R., Levendale, A., Watson, C. J., and Baugh, J. A. (2012) Hypoxia-induced DNA hypermethylation in human pulmonary fibroblasts is associated with Thy-1 promoter methylation and the development of a pro-fibrotic phenotype. *Respir Res* 13, 74.

15. Dutta, B., Adav, S. S., Koh, C. G., Lim, S. K., Meshorer, E., and Sze, S. K. (2012) Elucidating the temporal dynamics of chromatin-associated protein release upon DNA digestion by quantitative proteomic approach. *J Proteomics* 75, 5493-5506.

16. Hanahan, D., and Weinberg, R. A. (2000) The hallmarks of cancer. Cell 100, 57-70.

17. Thiery, J. P. (2002) Epithelial-mesenchymal transitions in tumour progression. *Nat Rev Cancer* 2, 442-454.

18. Park, J. E., Tan, H. S., Datta, A., Lai, R. C., Zhang, H., Meng, W., Lim, S. K., and Sze, S. K. (2010) Hypoxic tumor cell modulates its microenvironment to enhance angiogenic and metastatic potential by secretion of proteins and exosomes. *Mol Cell Proteomics* 9, 1085-1099.

19. Ren, Y., Hao, P., Dutta, B., Cheow, E. S., Sim, K. H., Gan, C. S., Lim, S. K., and Sze, S. K. (2013) Hypoxia modulates A431 cellular pathways association to tumor radioresistance and enhanced migration revealed by comprehensive proteomic and functional studies. *Mol Cell Proteomics* 12, 485-498.

20. Chaplin, D. J., Olive, P. L., and Durand, R. E. (1987) Intermittent blood flow in a murine tumor: radiobiological effects. *Cancer Res* 47, 597-601.

21. Johnson, A. B., Denko, N., and Barton, M. C. (2008) Hypoxia induces a novel signature of chromatin modifications and global repression of transcription. *Mutat Res* 640, 174-179.

22. Young, S. D., Marshall, R. S., and Hill, R. P. (1988) Hypoxia induces DNA over replication and enhances metastatic potential of murine tumor cells. *Proc Natl Acad Sci U S A* 85, 9533-9537.

23. Bristow, R. G., and Hill, R. P. (2008) Hypoxia and metabolism. Hypoxia, DNA repair and genetic instability. *Nat Rev Cancer* 8, 180-192.

24. Coquelle, A., Toledo, F., Stern, S., Bieth, A., and Debatisse, M. (1998) A new role for hypoxia in tumor progression: induction of fragile site triggering genomic rearrangements and formation of complex DMs and HSRs. *Mol Cell* 2, 259-265.

25. Rice, G. C., Hoy, C., and Schimke, R. T. (1986) Transient hypoxia enhances the frequency of dihydrofolate reductase gene amplification in Chinese hamster ovary cells. *Proc Natl Acad Sci U S A* 83, 5978-5982.

26. Thadani, R., Uhlmann, F., and Heeger, S. (2012) Condensin, chromatin crossbarring and chromosome condensation. *Curr Biol* 22, R1012-1021.

27. Schneider, K., Fuchs, C., Dobay, A., Rottach, A., Qin, W., Wolf, P., Alvarez-Castro, J. M., Nalaskowski, M. M., Kremmer, E., Schmid, V., Leonhardt, H., and Schermelleh, L. (2013) Dissection of cell cycle-dependent dynamics of Dnmt1 by FRAP and diffusion-coupled modeling. *Nucleic Acids Res* 41, 4860-4876.

28. Mizuno, S., Yasuo, M., Bogaard, H. J., Kraskauskas, D., Natarajan, R., and Voelkel, N. F. (2011) Inhibition of histone deacetylase causes emphysema. *Am J Physiol Lung Cell Mol Physiol* 300, L402-L413.

29. Toh, Y., and Nicolson, G. L. (2009) The role of the MTA family and their encoded proteins in human cancers: Molecular functions and clinical implications. *Clin Exp Metastasis* 26, 215-227.

30. Lim, J. H., Choi, Y. J., Cho, C. H., and Park, J. W. (2012) Protein arginine methyltransferase 5 is an essential component of the hypoxia-inducible factor 1 signaling pathway. *Biochem Biophys Res Commun* 418, 254-259.

31. Agrawal, S., Hofmann, W. K., Tidow, N., Ehrich, M., van den Boom, D., Koschmieder, S., Berdel, W. E., Serve, H., and Muller-Tidow, C. (2007) The C/EBPdelta tumor suppressor is silenced by hypermethylation in acute myeloid leukemia. *Blood* 109, 3895-3905.

32. Riley, T., Sontag, E., Chen, P., and Levine, A. (2008) Transcriptional control of human p53-regulated genes. *Nat Rev Mol Cell Biol* 9, 402-412.

33. Chen, D., Reierstad, S., Fang, F., and Bulun, S. E. (2011) JunD and JunB integrate prostaglandin E2 activation of breast cancer-associated proximal aromatase promoters. *Mol Endocrinol* 25, 767-775.

34. Abdul-Hafez, A., Shu, R., and Uhal, B. D. (2009) JunD and HIF-1alpha mediate transcriptional activation of angiotensinogen by TGF-beta1 in human lung fibroblasts. *FASEB J* 23, 1655-1662.

35. Lv, J., Liu, H., Wang, Q., Tang, Z., Hou, L., and Zhang, B. (2003) Molecular cloning of a novel human gene encoding histone acetyltransferase-like protein involved in transcriptional activation of hTERT. *Biochem Biophys Res Commun* 311, 506-513.

36. Liu, H., Ling, Y., Gong, Y., Sun, Y., Hou, L., and Zhang, B. (2007) DNA damage induces N-acetyltransferase NAT10 gene expression through transcriptional activation. *Mol Cell Biochem* 300, 249-258.

37. Nijwening, J. H., Geutjes, E. J., Bernards, R., and Beijersbergen, R. L. (2011) The histone demethylase Jarid1b (Kdm5b) is a novel component of the Rb pathway and associates with E2f-target genes in MEFs during senescence. *PLoS One* 6, e25235.

38. Dutta, B., Ren, Y., Hao, P., Sim, K. H., Cheow, E. S., Adav, S., Tam, J. P., and Sze, S. K. (2014) Profiling of the chromatin-associated proteome identifies HP1BP3 as a novel regulator of cell cycle progression. Mol. Cell. Proteomics doi: 10.1074/mcp.M113.034975 mcp.M113.034975".

39. Schmaltz, C., Hardenbergh, P. H., Wells, A., and Fisher, D. E. (1998) Regulation of proliferation-survival decisions during tumor cell hypoxia. *Mol Cell Biol* 18, 2845-2854.

40. Gumbiner, B. M. (1996) Cell adhesion: the molecular basis of tissue architecture and morphogenesis. *Cell* 84, 345-357.

41. Schlie-Wolter, S., Ngezahayo, A., and Chichkov, B. N. (2013) The selective role of ECM components on cell adhesion, morphology, proliferation and communication in vitro. *Exp Cell Res* 319, 1553-1561.

42. Hynes, R. O., and Lander, A. D. (1992) Contact and adhesive specificities in the associations, migrations, and targeting of cells and axons. *Cell* 68, 303-322.

43. Phillips-Mason, P. J., Craig, S. E., and Brady-Kalnay, S. M. (2011) Should I stay or should I go? Shedding of RPTPs in cancer cells switches signals from stabilizing cell-cell adhesion to driving cell migration. *Cell Adh Migr* 5, 298-305.

44. Kumareswaran, R., Ludkovski, O., Meng, A., Sykes, J., Pintilie, M., and Bristow, R. G. (2012) Chronic hypoxia compromises repair of DNA double-strand breaks to drive genetic instability. *J Cell Sci* 125, 189-199.

45. Huang, L. E., Bindra, R. S., Glazer, P. M., and Harris, A. L. (2007) Hypoxia-induced genetic instability--a calculated mechanism underlying tumor progression. *J Cell Mol Med* 85, 139-148.

46. Banath, J. P., Sinnott, L., Larrivee, B., MacPhail, S. H., and Olive, P. L. (2005) Growth of V79 cells as xenograft tumors promotes multicellular resistance but does not increase spontaneous or radiation-induced mutant frequency. *Radiat Res* 164, 733-744.

47. Lieber, M. R. (2010) The mechanism of double-strand DNA break repair by the nonhomologous DNA end-joining pathway. *Annu Rev Biochem* 79, 181-211.

48. Takashima, Y., Sakuraba, M., Koizumi, T., Sakamoto, H., Hayashi, M., and Honma, M. (2009) Dependence of DNA double strand break repair pathways on cell cycle phase in human lymphoblastoid cells. *Environ Mol Mutagen* 50, 815-822.

49. Keith, B., and Simon, M. C. (2007) Hypoxia-inducible factors, stem cells, and cancer. *Cell* 129, 465-472.

50. Mazumdar, J., Dondeti, V., and Simon, M. C. (2009) Hypoxia-inducible factors in stem cells and cancer. *J Cell Mol Med* 13, 4319-4328.

51. Bao, B., Ahmad, A., Kong, D., Ali, S., Azmi, A. S., Li, Y., Banerjee, S., Padhye, S., and Sarkar, F. H. (2012) Hypoxia induced aggressiveness of prostate cancer cells is linked with deregulated expression of VEGF, IL-6 and miRNAs that are attenuated by CDF. *PloS one* 7, e43726.

52. Wang, X., Liu, Q., Hou, B., Zhang, W., Yan, M., Jia, H., Li, H., Yan, D., Zheng, F., Ding, W., Yi, C., and Hai, W. (2013) Concomitant targeting of multiple key transcription factors effectively disrupts cancer stem cells enriched in side population of human pancreatic cancer cells. *PloS one* 8, e73942.

Supplemental Figures:

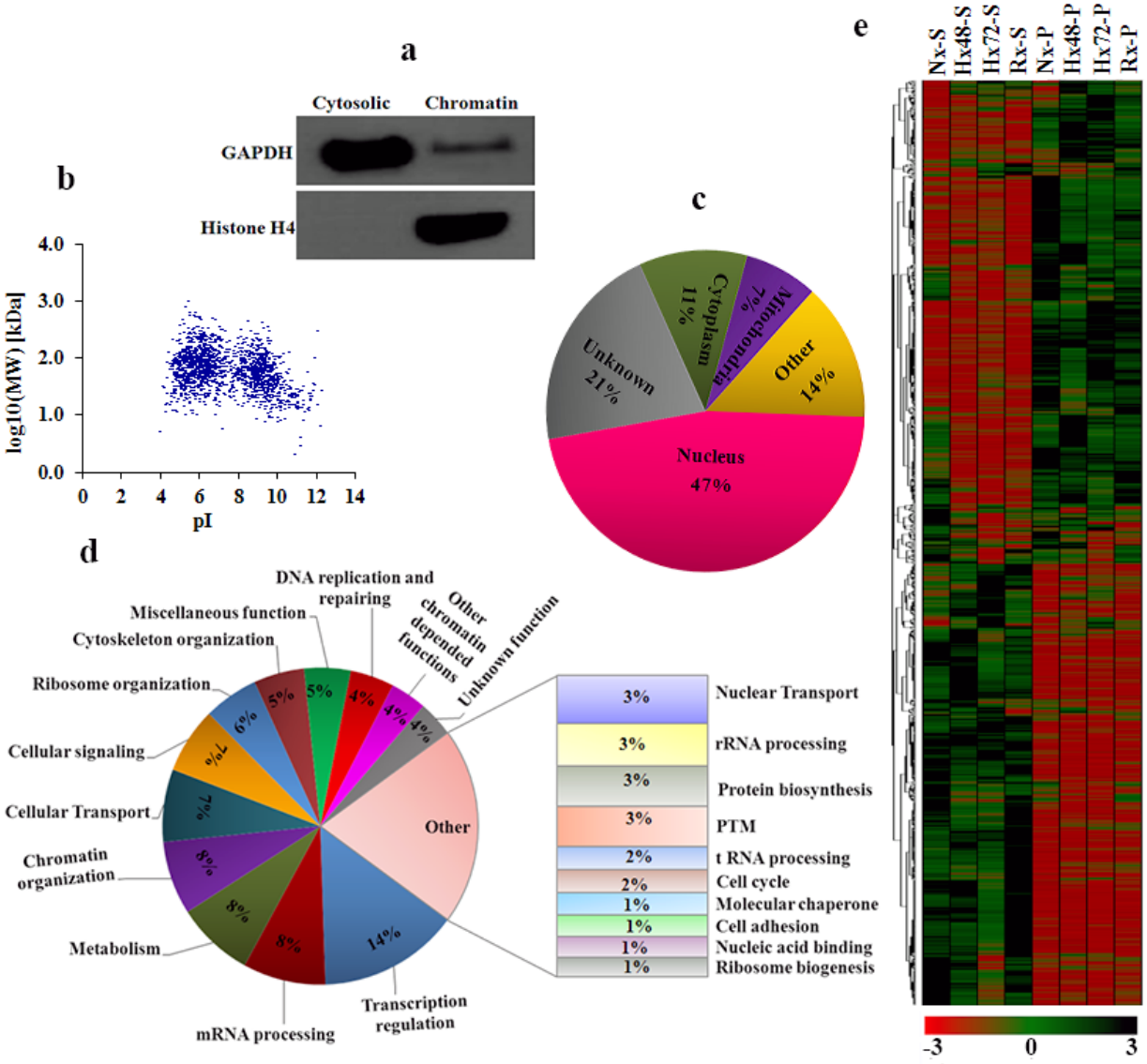

Figure S1: Characterization of identified proteins. a: Western blot of GAPDH and histone H4 in cytosolic and chromatin fractions respectively. b: Physicochemical distribution of the identified proteins according to molecular weight (MW) and isoelectric point (pI). c: Classification of the identified proteins according to their subcellular localization. d: Functional classification of the identified proteins. e: Heat-map showing relative protein abundance in the different chromatin digests. iTRAQ values of different chromatin digests were used for the cluster analysis.

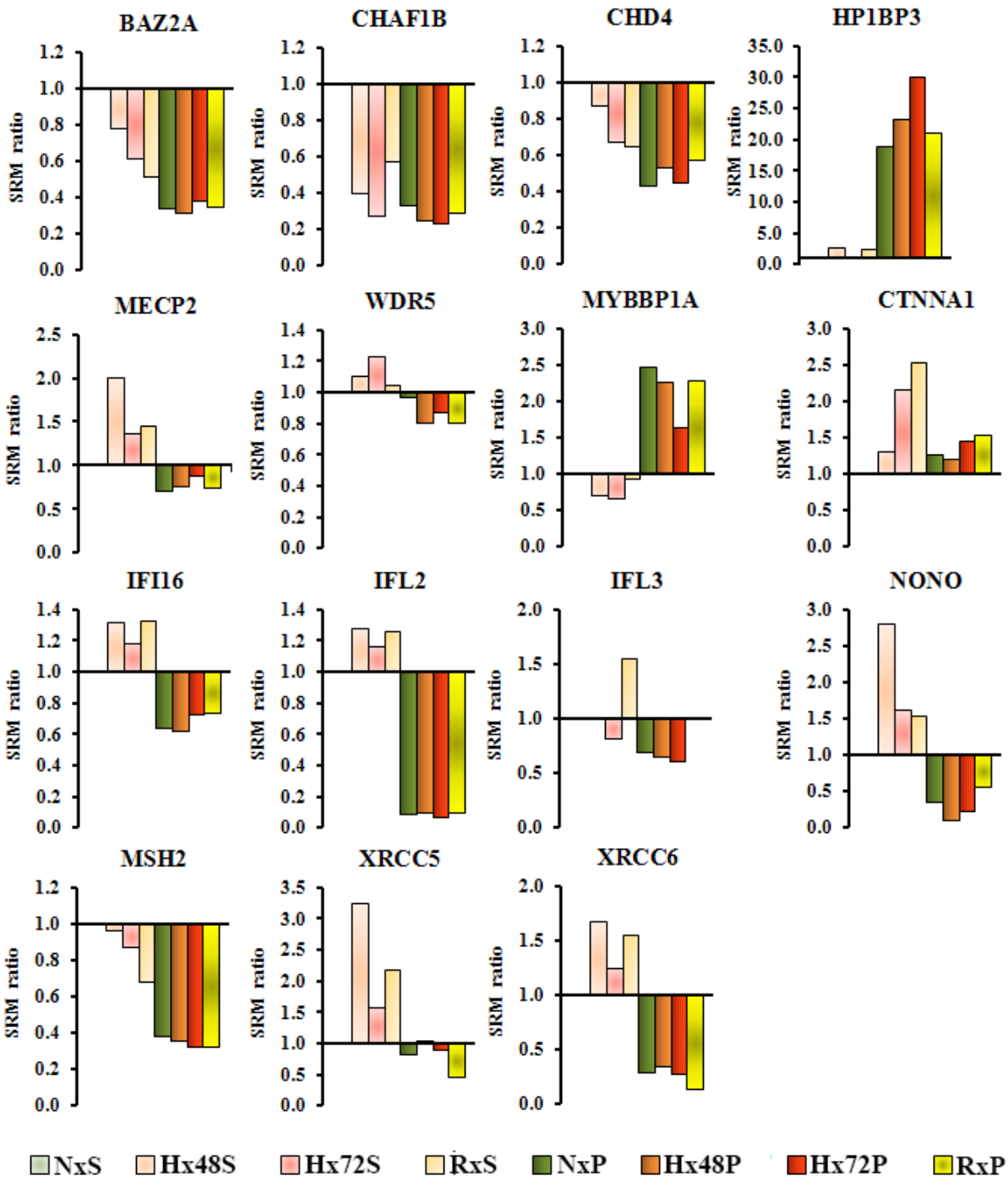

Figure S2: Validation of quantitative iTRAQ results by SRM based quantification. SRM ratio represents the relative protein abundance in different nuclease digests. Chromatins from different conditions were partially digested by DNase I and proteins were quantified by SRM based proteomic approach. Supernatant fractions Nx-S, Hx48-S, Hx72-S and Rx-S and pellet fractions Nx-P, Hx48-P, Hx72-P and Rx-P were obtained by partial DNase I digestion of respective chromatin extracted from normoxic, 48h hypoxic, 72h hypoxic and reoxygenated A431 cells.

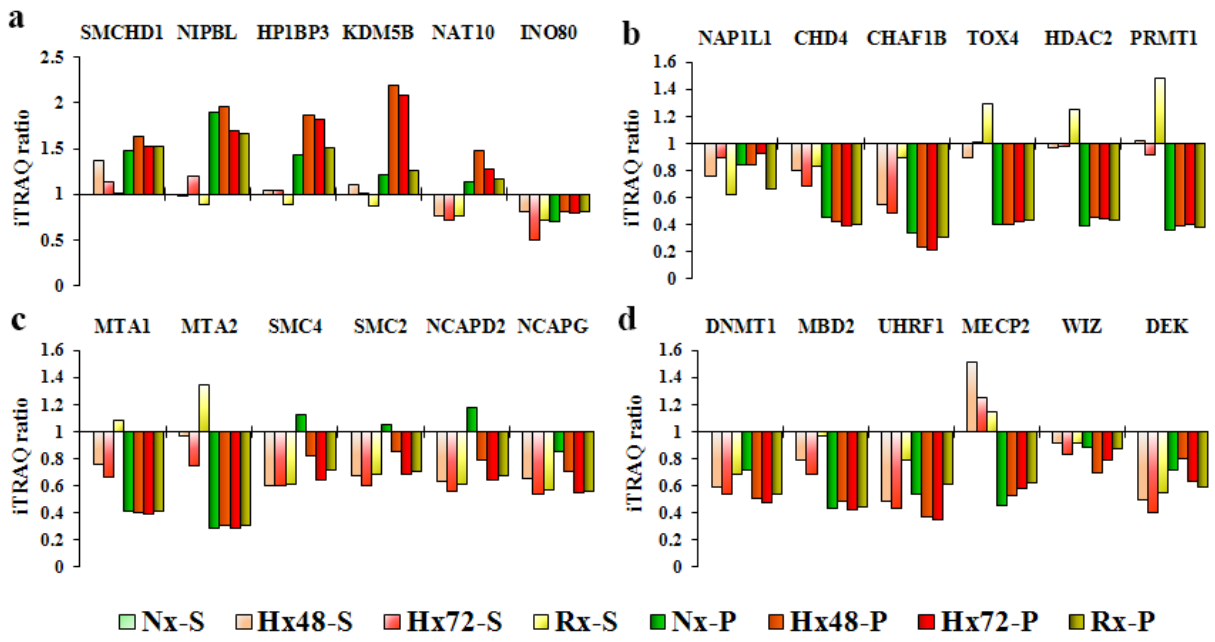

Figure S3: Chromatin organizer proteins exhibit differential association with chromatin during hypoxia and re-oxygenation. A431 cancer cells were cultured under conditions of normoxia (Nx), 48h hypoxia (Hx48), 72h hypoxia (Hx72), or 48h hypoxia followed by 24h re-oxygenation (Rx). Chromatin was then extracted from the cells and subjected to partial DNase I digestion to release euchromatin-binding proteins into the supernatant (suffix S) and leave heterochromatin-bound proteins behind in the undigested pellet (suffix P). Shown are iTRAQ ratios indicating the relative abundance of proteins in the different chromatin digests (a-d).

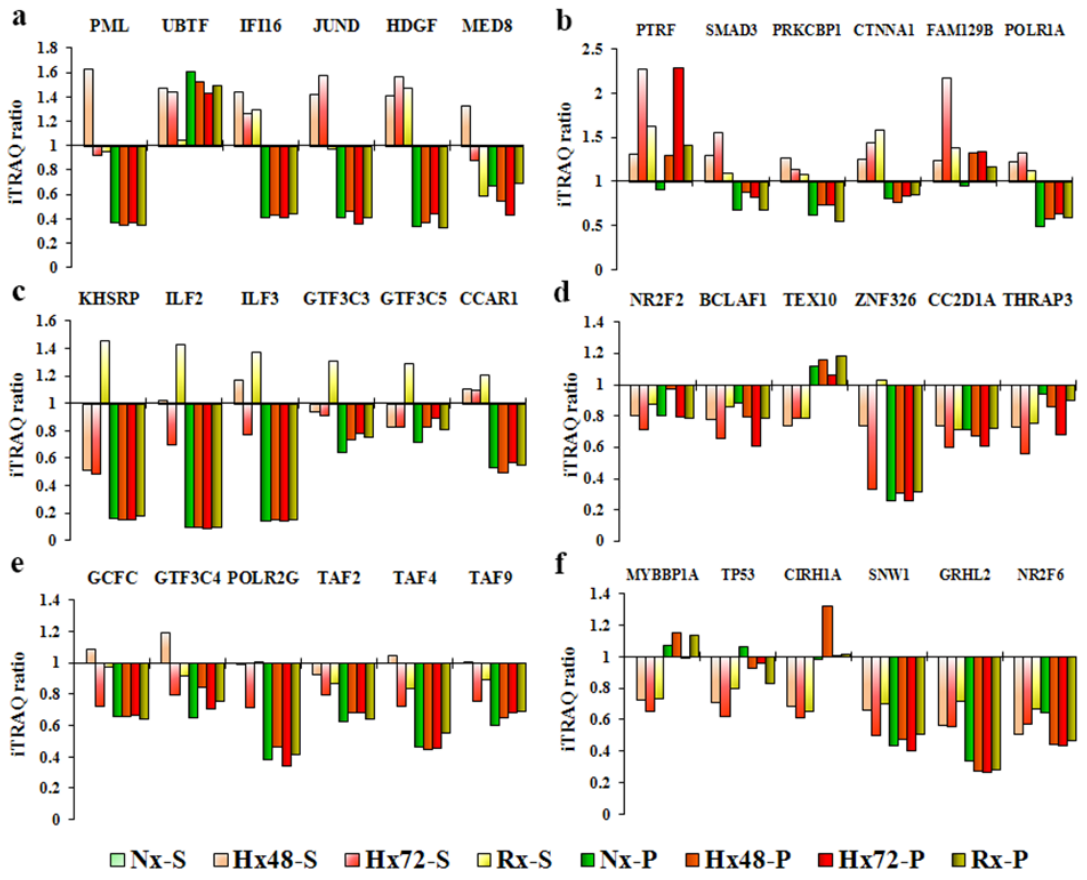

Figure S4: Chromatin association of transcriptional regulators is modulated by hypoxia/re-oxygenation. A431 cancer cells were cultured under conditions of normoxia (Nx), 48h hypoxia (Hx48), 72h hypoxia (Hx72), or 48h hypoxia followed by 24h re-oxygenation (Rx). Chromatin was then extracted from the cells and subjected to partial DNase I digestion to release euchromatin-binding proteins into the supernatant (suffix S) and leave heterochromatin-bound proteins behind in the undigested pellet (suffix P). Shown are iTRAQ ratios indicating the relative abundance of proteins in the different chromatin digests (a-f).

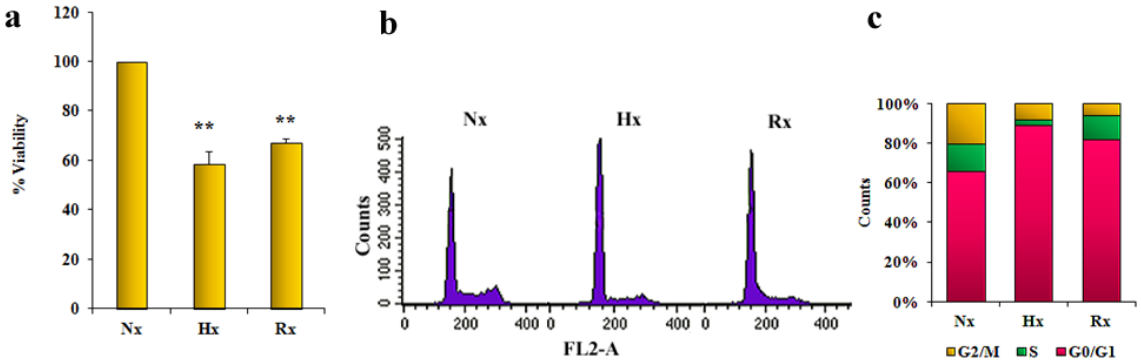

Figure S5: Viability and cell cycle progression of A431 cells under hypoxic conditions. a: Percentage of viable A431 cells as assessed by MTT assay after culture in normoxia, hypoxia, or hypoxia/re-oxygenation (n=3 biological replicates, **P<0.005). b: Cell cycle analysis of normoxic, hypoxic and re-oxygenated cells after staining with propidium iodide and measurement of DNA content using flow-cytometry. c: Phase distribution of cells cultured under normoxic, hypoxic or re-oxygenated conditions.

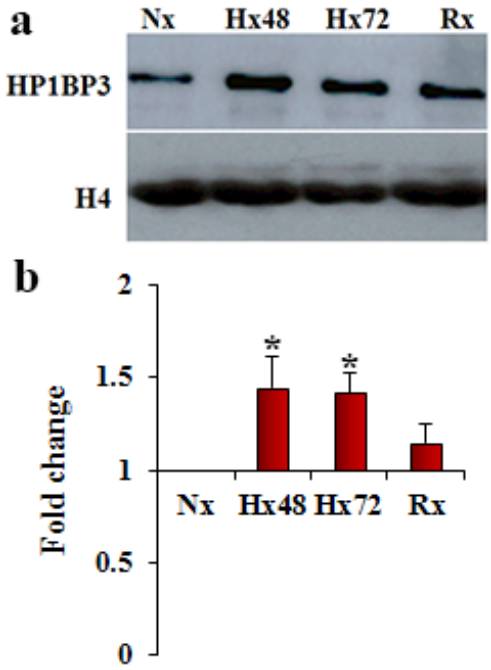

Figure S6: Chromatin association of HP1BP3 during different hypoxic conditions. a: Western blot images showing the differential association of HP1BP3 with chromatin during hypoxia and re-oxygenation. Chromatin extract from different conditions were used for the western blot analysis. b: Change in HP1BP3 chromatin association level under variable oxygenation. The chromatin association level of HP1BP3 is expressed relative to that of histone 4 (n=5 experimental replicates, *P<0.05).

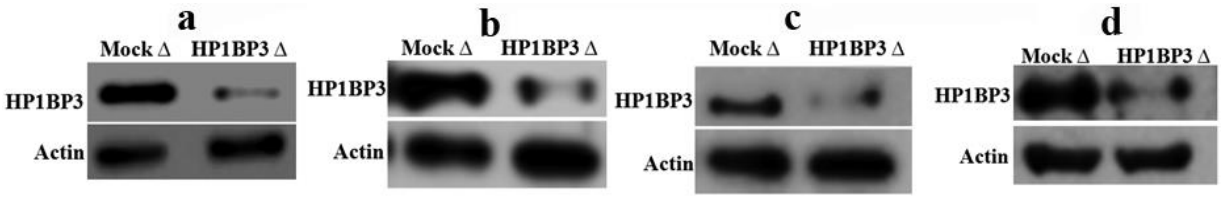

Figure S7: Confirmation of HP1BP3 knockdown. Western blots confirming successful shRNA-knockdown of HP1BP3 expression in A431 cancer cells using shRNA-1(a), shRNA-2 (b) and shRNA-3(c). HP1BP3 knockdown in U2OS cells using shRNA-1(d).

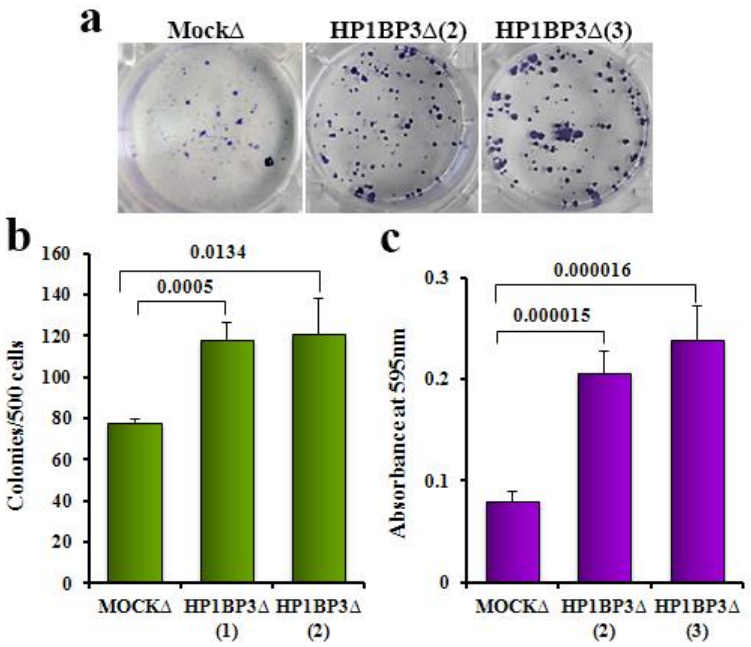

Figure S8: Validation of on target effect of HP1BP3 shRNA during clonogenic assay. Representative images (a) and quantification of crystal violet staining in HP1BP3-depleted A431 phenotypes obtain by using shRNA-2 and shRNA-3 and mock-depleted control cells (b and c). Each experiment was performed in triplets.

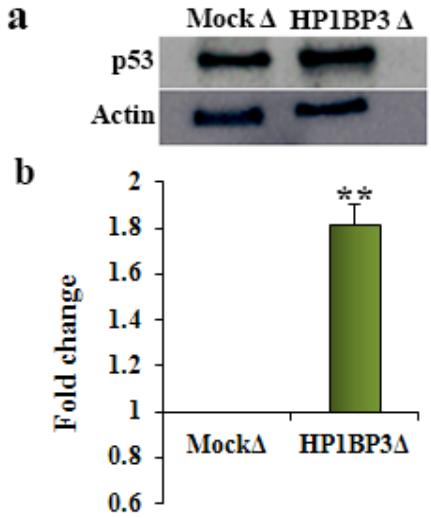

Figure S9: HP1BP3 depletion is associated with increased p53 expression in A431 cells. a: Analysis of p53 expression level in HP1BP3-depleted A431 cells and mock-depleted control cells by Western blot (a) or quantification expressed relative to actin staining (b) (n=5 experimental replicates, **P<0.005).

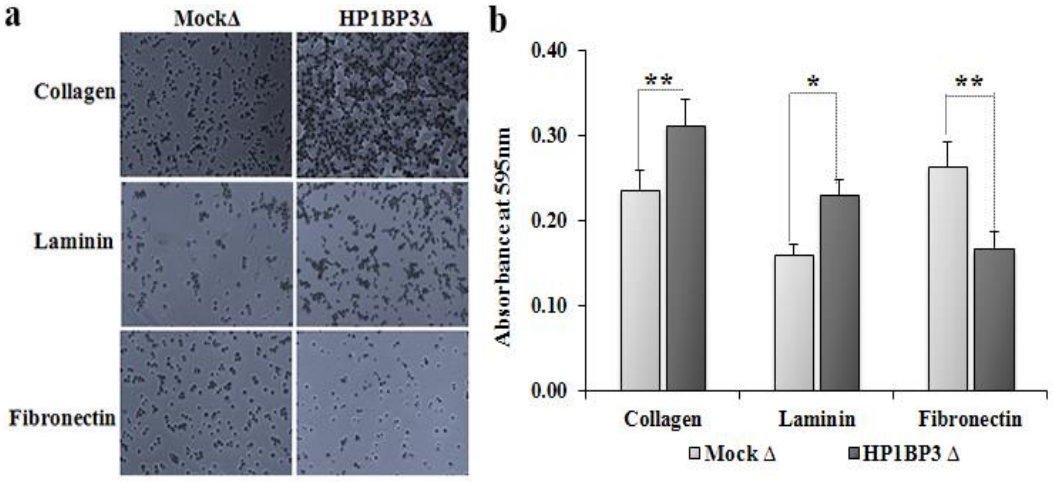

Figure S10: HP1BP3-mediated regulation of cell adhesion. Adhesion of HP1BP3-depleted A431 cells to ECM proteins collagen, laminin or fibronectin, compared with mock-depleted control cells (*P<0.05, **P<0.005).

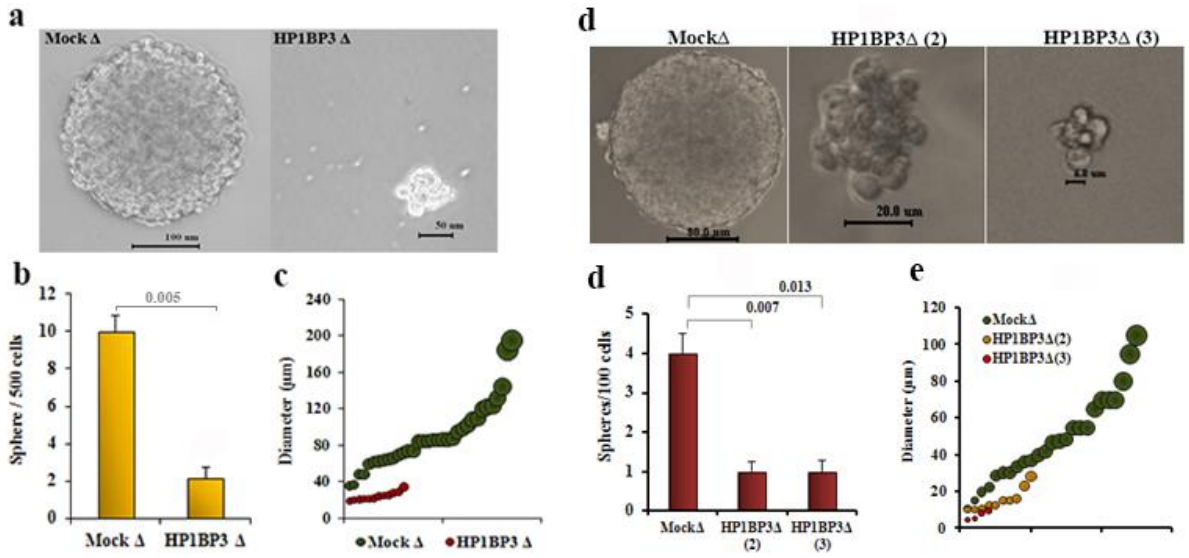

Figure S11: HP1BP3 depletion impairs cancer cell self-renewal. a: Images of tumor spheres formed by HP1BP3-depleted different A431 phenotypes obtained by using different shRNAs (HP1BP3Δ [shRNA-1], HP1BP3Δ(2) [shRNA-2] and HP1BP3Δ(3) [shRNA-3]) or mock-depleted controls(a). Number of tumor spheres formed/specified number of cells seeded (b and d). Size distribution of tumor spheres formed by HP1BP3 depleted A431 phenotypes and mock control A431 cells (c and e). Each experiment was performed in triplets.

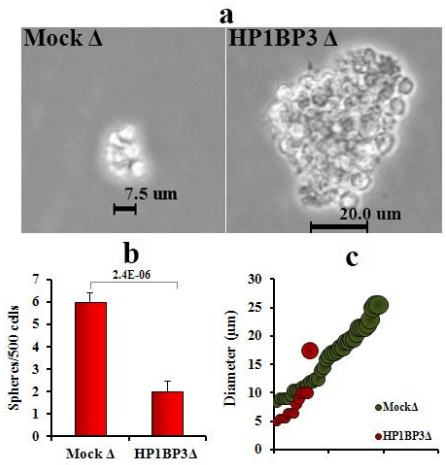

Figure S12: Effect of HP1BP3 depletion upon self-renewal property of U2OS cells. a: Images of spheres formed by mock and HP1BP3 depleted U2OS cells. b: Number of tumorospheres formed/500 cells seeded c: Size distribution of mock and HP1BP3 depleted U2OS spheres. Each experiment was performed in triplets.

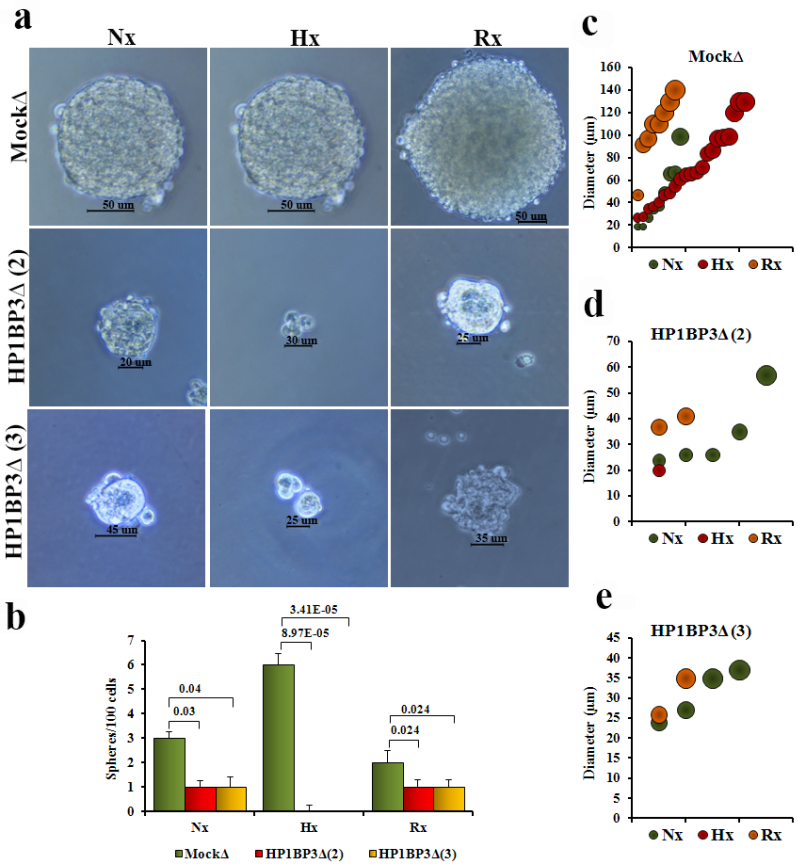

Figure S13: Effect of HP1BP3 depletion upon self-renewal property of cancer cells during hypoxia/re-oxygenation. HP1BP3-depleted A431 cells were cultured for 48h in normoxia (Nx), 48h hypoxia (Hx), or 24h hypoxia/24h re-oxygenation (Rx), and then assessed for tumor sphere formation over 10d of culture (a and b). Size distribution of tumor spheres formed by HP1BP3-depleted A431 cells subjected to the same conditions (c-e). Each experiment was performed in triplets. Different HP1BP3 depleted phenotypes were obtained from stable transfection of different shRNAs (shRNA-2 and shRNA-3) in A431 cells.

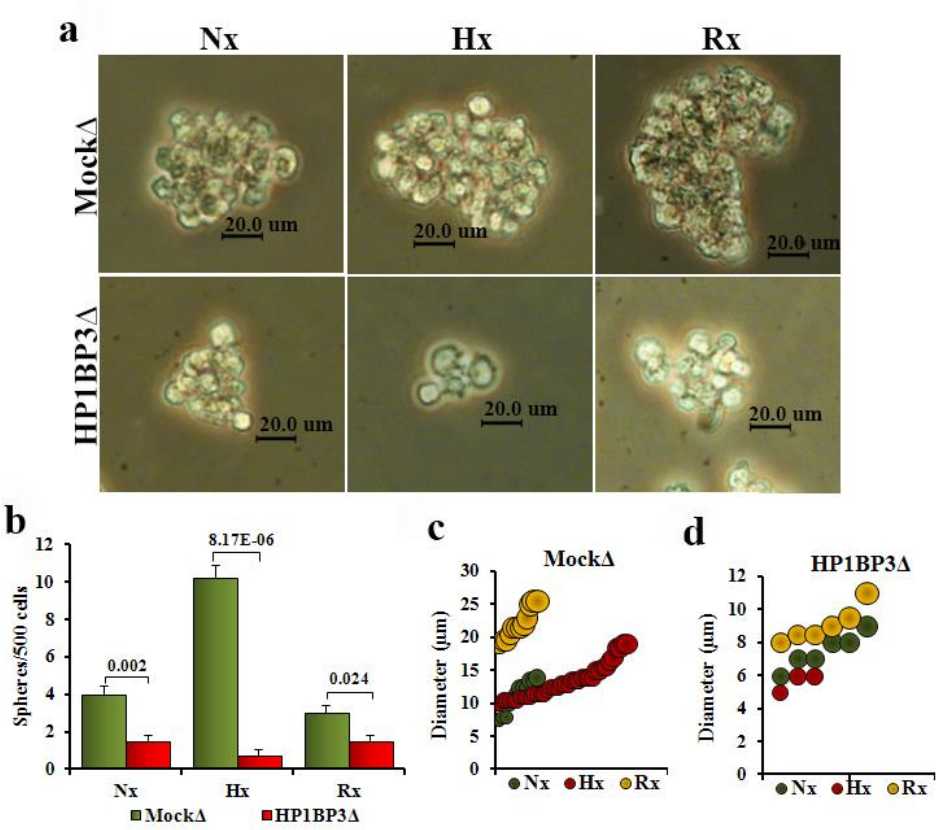

Figure S14: HP1BP3 depletion inhibits self-renewal property of U2OS cells during hypoxia/re-oxygenation. HP1BP3-depleted U2OS cells were cultured for 48h in normoxia (Nx), 48h hypoxia (Hx), or 24h hypoxia/24h re-oxygenation (Rx), and then assessed for tumor sphere formation over 10d of culture (a and b). Size distribution of tumor spheres formed by HP1BP3-depleted U2OS cells subjected to the same conditions (c). Each experiment was performed in triplets.

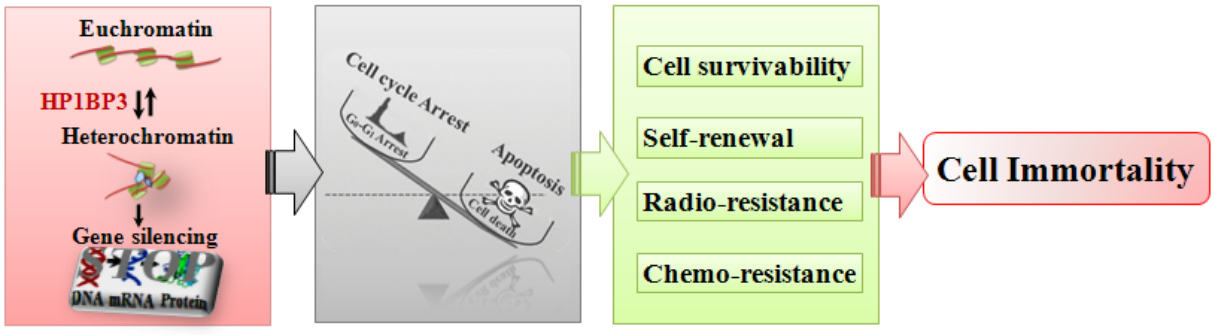

Figure S15: HP1BP3-induced immortalization of cancer cells during hypoxia.